JGR Oceans

RESEARCH ARTICLE
10.1029/2020JC016317

Key Points:

- Assessment of an eddying 1/12° ocean reanalysis with non-assimilated hydrographic observations along 59.5°N in the Atlantic
- Reliable representation of the 0–700 m heat content but flaws in overflow waters due to a lack of deep observations
- Reliable reproduction outside the western boundary current of the major mesoscale eddy features contributing to the meridional transport

Supporting Information:

Supporting Information may be found in the online version of this article.

Correspondence to:

P. Verezemskaya,
verezem@sail.msk.ru

Citation:

Verezemskaya, P., Barnier, B., Gulev, S. K., Gladyshev, S., Molines, J.-M., Gladyshev, V., et al. (2021). Assessing eddying (1/12°) ocean reanalysis GLORYS12 using the 14-yr instrumental record from 59.5°N section in the Atlantic. *Journal of Geophysical Research: Oceans*, *126*, e2020JC016317. https://doi.org/10.1029/2020JC016317

Received 10 APR 2020
Accepted 27 MAY 2021

Assessing Eddying (1/12°) Ocean Reanalysis GLORYS12 Using the 14-yr Instrumental Record From 59.5°N Section in the Atlantic

Polina Verezemskaya[1], Bernard Barnier[1,2], Sergey K. Gulev[1], Sergey Gladyshev[1], Jean-Marc Molines[2], Vsevolod Gladyshev[1], Jean-Michel Lellouche[3], and Alexander Gavrikov[1]

[1]P.P. Shirshov Institute of Oceanology, Russian Academy of Science, Moscow, Russia, [2]Institut des Géosciences de l'Environnement, Université Grenoble Alpes, CNRS, IRD, Grenoble, France, [3]Mercator Ocean International, Ramonville Saint Agne, France

Abstract The eddy-resolving (1/12°) global ocean reanalysis GLORYS12 is assessed against 14 years (2002–2015) of independent hydrographic observations collected at 59.5°N in the North Atlantic. Two multi-observations statistical analyses, ISAS-15 and ARMOR-3D, and an eddy-permitting (1/4°) reanalysis, GLORYS025, also contribute to this comparison. The mean thermohaline structure along the 59.5°N section revealed by the observations is well-reproduced by GLORYS12, except for the overflow waters. A good agreement with observations is found for linear trends over the whole period, exhibiting a dipole-like pattern with a cooling/freshening in the main thermocline and a warming/salinization below. However, localized discrepancies with observations suggest the need for improvement in the reanalysis system (especially in the overflows representation and the consistency between the forcing and data assimilation system) and the deep observational array. The reanalysis reliably represents the ocean heat content in the upper 700-m layer but shows significant differences with observations between 700 and 2,000 m. The meridional volume and heat transports across the 59.5°N section are compared for years when ADCP observations were available. The reanalysis does not reproduce the variability observed in the western boundary current but agrees well with observed transports in the other parts of the section. The reanalysis reproduces the major mesoscale eddy features that contribute to the meridional transport and provides the large-scale context of their location. The analysis of time correlation at all measurement points demonstrated that GLORYS12 is the most accurate among the analyzed datasets used in this study to represent and explain the observed ocean characteristics and variability along that section.

Plain Language Summary The GLORYS12 reanalysis data set produced recently by Mercator Ocean International forecasting center describes the day-to-day evolution of the world-ocean physical properties for 1993–2018. This reanalysis uses many observations of different kinds to constrain the solution of a dynamical ocean forecasting model. GLORYS12 is assessed against 14 years of hydrographic (temperature and salinity) observations, not used in the reanalysis process, collected annually between Scotland and Greenland along 59.5°N. The observed time-mean thermohaline structure and patterns of the temporal trends along 59.5°N are well represented except for the deep waters of Arctic origin that flows along Greenland. Local discrepancies between reanalysis and observations emphasize the need for improvements in the reanalysis system and observations at depth. GLORYS12 provides a reliable assessment of the ocean heat content in the upper 700 m, an important climate index, the agreement which deteriorates at greater depths. The comparison with similar datasets produced by statistical analyses of observations (not using a dynamical model) shows that GLORYS12 is the one that best describes the variability seen in the observations. The reanalysis, because it provides a view of the large-scale circulation context, allows to relate the variability of the meridional heat transport across the section to the presence of mesoscale circulation features.

1. Introduction

Ocean reanalyzes (ORAs) provide estimates of the long-term evolution of the ocean state. They supply users with high-resolution ocean physical and biogeochemical characteristics at the global and regional scales over several decades. The detailed strategy of the development of ocean reanalyzes and the overview of the

major global reanalyzes involved in the CLIVAR/GODAE Ocean Reanalysis Intercomparison project (ORA-IP) are presented in, for example, Balmaseda et al. (2015) and Masina et al. (2015), Storto et al. (2019)and von Schuckmann et al. (2019). ORAs combine different ocean observations (in-situ and satellite) with the solution of a state-of-the-art ocean general circulation model via optimal data assimilation methods. Similar to atmospheric reanalyzes, ORAs have the potential to provide more internally consistent and accurate estimates of the ocean state and its variability compared to the estimates solely based on observations or free (non-assimilated) model simulations, especially when the eddying ocean is considered (Masina et al., 2015).

While early ORAs did not use all available observations (Balmaseda et al., 2015; Carton et al., 2018, 2019) due to the limitations imposed by the data assimilation techniques, the recent ORAs largely benefit from the advanced data assimilation methods that allow for the use of a variety of ocean observations (Lellouche et al., 2018; Zuo et al., 2015, 2019). These include (while not limited to) the in-situ databases such as CORA (Cabanes et al., 2013) and EN4 (Good et al., 2013), ARGO floats data (Roemmich and the Argo Steering Team, 2009), satellite observations of sea level anomalies like AVISO (https://www.aviso.altimetry.fr) and improved sea surface temperature (SST) datasets like AVHRR or OSTIA (Donlon et al., 2012). In this respect, the assessment of the ORAs using independent observations (those not being assimilated) is a challenge.

ORAs are used mainly for climate monitoring studies, focusing on the ocean temperature and salinity variability on a decadal time scale (Carton et al., 2018, 2019), ocean heat content (Balmaseda et al., 2013; Meyssignac et al., 2019; Palmer et al., 2017; Xue et al., 2012), the steric sea level variability (Storto et al., 2017), the assessment of the upper ocean salinity content (Shi et al., 2017), or air-sea fluxes and ocean-associated global energy imbalances (Valdivieso et al., 2017, von Schuckmann et al. 2016a). ORAs are used in the Ocean State Reports of the Copernicus Marine Environment Monitoring Service (CMEMS, http://marine.copernicus.eu/) to document the evolution of several climate essential variables, changes in ocean climate, and to report on the extreme ocean or sea-ice conditions (von Schuckmann et al., 2016b, 2019; von Schuckmann, 2018).

However, most studies cited above did not use independent data to assess the ORAs, but rather employed a large number of existing ORAs for implementing multi-reanalysis ensemble approaches for improving the estimation of signals and quantifying uncertainties in individual ORAs using signal-to-noise ratio (Balmaseda et al., 2015; Masina et al., 2015; Storto et al., 2017 among others). Many of these studies clearly demonstrated serious flaws in ORAs and posed several fundamental open questions about the robustness of the reanalyzed ocean characteristics. This justifies the necessity of continuous efforts for assessing the quality of ORAs in order to improve further models, assimilation techniques, and observing systems. In this regard, observations, which are not assimilated in ORAs, are of a special value, especially when they cover periods from several years to decades.

This paper is focused on the regional assessment of the recent GLORYS12 Version 1 reanalysis (GLORYS12 hereafter), the first eddy-resolving (1/12°) global ORA produced by Mercator Ocean International (https://www.mercator-ocean.fr/en/). We focus on the representation of the circulation phenomena revealed by observations at the transatlantic section along 59.5°N (referred to as the 59.5°N section hereafter) between Greenland and Scotland. This approach is grounded by the availability of the long-term in-situ hydrographic observations collected annually from 1997 onwards along 59.5°N by the IORAS (Shirshov Institute of Oceanology, Moscow). While extensively used in different regional oceanographic studies (Falina et al. 2007; Gladyshev et al. 2018, 2019; Sarafanov et al. 2008, 2010), this data set has not been assimilated in the present ORAs and thus represents a unique opportunity to validate GLORYS12 against truly independent observations in a critically important ocean region. Therefore, we limit our assessment to the ability of the GLORYS12 reanalysis to represent the state of the ocean along 59.5°N as revealed by the hydrographic observations over the period 2002–2015. The products used in this study are described in Section 2. Section 3 describes the pre-processing applied to the data and also the metrics used for validation. The assessment of GLORYS12 at 59.5°N is presented in Section 4. Conclusive Section 5 provides the discussion and gives the outlook of the validation of GLORYS12.

2. Products Used in the Study

2.1. GLORYS12 Ocean Global Reanalysis

GLORYS12 is a global ocean eddy-resolving ORA covering the satellite altimetry era 1993–2018 produced by Mercator Ocean International in the context of the CMEMS. The reanalysis system is largely based on the current real-time global CMEMS forecasting system (Lellouche et al., 2018), which employs the ocean and sea-ice circulation model ORCA12 (DRAKKAR Group, 2014), global implementation of the NEMO platform (Madec et al., 2016). The model horizontal grid is quasi-isotropic with a resolution of 1/12° (9.25 km at the equator and ∼4.5 km at subpolar latitudes) and 50 vertical levels, with the spacing increasing with depth (22 are within the first 100 m). In GLORYS12, the ocean model is driven at the surface by the European Center for Medium-Range Weather Forecasts (ECMWF) ERA-Interim atmospheric reanalysis (Dee et al., 2011). A 3-h sampling of atmospheric quantities is used to reproduce the diurnal cycle. Due to largely known biases in precipitations and radiative fluxes at the surface, a satellite-based large-scale correction is applied to the ERA-Interim fluxes (Garric et al., 2018). A multivariate reduced-order Kalman filter is used to assimilate different types of observations in a 7-day assimilation cycle (Lellouche et al., 2018). Along track altimeter sea level anomalies (Pujol et al., 2016), AVHRR satellite sea surface temperature from NOAA, Ifremer/CERSAT sea-ice concentration (Ezraty et al., 2007), and in situ temperature and salinity vertical profiles from the latest CORA in situ databases (Cabanes et al., 2013; Szekely et al., 2016) are jointly assimilated. No satellite salinity products were assimilated. A "hybrid" Mean Dynamic Topography (MDT) has also been used as a reference for altimeter data assimilation. This hybrid MDT is based on the CNES-CLS13 MDT (Rio et al., 2014) with some adjustments (Hamon et al., 2019). No digital time filter is included in the SLA processing. In parallel with the multivariate reduced-order Kalman filter, GLORYS12 employs a 3D-VAR scheme, which provides a correction for the slowly evolving large-scale biases in temperature and salinity. GLORYS12 reanalysis provides, among many parameters, daily 3D fields of temperature, salinity, and current velocity from top to bottom, complemented by sea surface height, mixed layer depth, and sea-ice parameters. In the present study, we use the period 2002–2015.

2.2. In-Situ Observations Along the 59.5°N Section

The first full-depth section along the 59.5°N IORAS section was carried out by the R/V "Professor Shtokman" in 1997. Then regular annual surveys (typically between June and September) have been conducted from 2002 to the present (Daniault et al., 2016, Gladyshev et al., 2016, 2017, 2018; Sarafanov et al., 2018). Until 2005, the distance between stations was 1-degree longitude (30 nautical miles). In 2006, the intra-station distance was reduced to 20 miles in the Icelandic basin and in the Irminger Sea. During the 2007 survey, the distance between stations was set to 15 miles, and since 2008 the maximum intra-station distance never exceeded 20 miles. Since 2009, the station spacing over the shelf and continental slope of Greenland in the region of the western boundary current system decreased to 2–10 miles. In 1997, 2002, and 2003 only CTD measurements were conducted. Single down-looking lowered ADCP WHS 300 kHz was used to measure currents in 2004–2006. Since 2007, a dual 300 kHz LADCP system (down and up-looking) was implemented, and from 2009 the continuous upper layer current measurements started using TRDI OS38 kHz and OS75 kHz shipboard ADCPs. In the present study, we use the temperature, and salinity profiles from the 14 annual cruises between 2002 and 2015 and further herein refer to this data set as OBS.

2.3. ARMOR-3D and ISAS-15 Multi-Observations-Based Datasets

We use the ARMOR-3D data set (ARMOR hereafter, Guinehut et al. [2012], Mulet et al., [2012]), which consists of global temperature, salinity, geopotential heights, and geostrophic currents on a 1/4° regular grid and on 33 depth levels from the surface down to 5,500 m. This data set is produced by combining satellite (sea level anomalies, geostrophic surface currents, sea surface temperature) and in-situ observations (temperature and salinity profiles) through a three-step statistical procedure. First, satellite observations of sea level anomalies and sea-surface temperature are projected onto the vertical via a multiple linear regression method using co-variances deduced from historical observations. This provides synthetic fields, which then, along with all available in-situ T/S profiles, are combined through an optimal interpolation method. This leads to the ARMOR T/S combined fields. Finally, the thermal wind equation with a reference level at

the surface is used to combine geostrophic surface current fields from satellite altimetry with ARMOR T/S fields to generate the global geostrophic current and geopotential height fields. ARMOR fields are available from CMEMS (CMEMS reference: MULTIOBS_GLO_PHY_REP_015_002) as weekly or monthly means for the period 1993–2018.

We also used the ISAS-15 product (In-Situ Analysis System, ISAS hereafter, Gaillard et al. [2016]; Kolodziejczyk et al. [2017]). It provides gridded fields of temperature and salinity between the surface and 2,000 m that preserve to the extent possible the time and space sampling capabilities of the network of ARGO profiling floats but also incorporates many different sources of the vertical profiles (gliders, XBT, sea mammals, etc.,). ISAS15 was not used for estimating the transport because it does not provide ocean current estimates. We also use monthly mean fields for the period 2002–2015. Note that ARMOR, ISAS, and GLORYS12 have many observations in common.

2.4. GLORYS025 Ocean Global Reanalysis

To better assess the value added by the high resolution of GLORYS12, we also use a previous eddy-permitting reanalysis performed by Mercator Ocean Intl. at a resolution of 1/4°. This reanalysis referred to here as GLORYS025 (the reference at Mercator Ocean is GLORYS2V4, also available from CMEMS under reference CMEMS-GLO-PUM-001-031) is very comparable to GLORYS12 in terms of assimilated observations and assimilation technique, the much noticeable difference being in the grid resolution of the model which is nine times coarser (1/4° vs. 1/12°). The main characteristics of the GLORYS025 reanalysis series are described in Ferry et al. (2010). GLORYS12 and GLORYS025 data were provided and analyzed on their original computational grids.

3. Methods

3.1. Data Processing

GLORYS12 reanalysis daily mean values of potential temperature, salinity, and current vectors for the period 2002–2015 over the subpolar North Atlantic (Figure 1) are provided on the original computational grid (1/12° or every 4.695 km along 59.5°N, and 50 vertical levels). Although the position of the section along which in-situ observations have been collected was maintained (at 59.5°N) from year to year, the location of the CTD stations varied (see Section 2.2). Therefore, a projection of the observations collected at all sections on a common grid is required to estimate their time mean properties and their year-to-year changes over the 14 years period. We chose to interpolate the observed in-situ profiles onto the 1/12° model grid because this latter grid is regular and has the finest resolution. We first calculated the mean path of the ship over 14 cruises. Then, the common grid of the section of resolution 1/12° is defined by taking the model grid points closest to the mean path. To project the observations on the common grid, a Gaussian weighted interpolation is used with a core size dependent on the distance between station locations (which slightly varies from year to year) and GLORYS12 grid points. This process does not degrade the high resolution of the reanalysis and does not add any information to the in-situ observations, and so allows for a quantitative comparison of the two datasets. Because it takes approximately 10 days to carry out the observational section, the observations do not provide an instantaneous view of the section. Therefore, we use the average of the GLORYS12 data over the section deployment period (∼10 days) to represent the section rather than a daily snapshot. We compared this co-location in time with the more accurate co-location at the exact time when the CTD profiles were made and found negligible discrepancies (i.e., the difference between the section sampled with the ∼10 days mean and that sampled with the exact time is an order of magnitude smaller than the differences between the reanalysis and the observations, see Supplementary Figure S1). This has the advantage of increasing the relevance of the comparison with the ARMOR data that have a weekly sampling.

For quantitative comparison, ISAS, ARMOR, and GLORYS025 data were interpolated from their original grid onto the common 1/12° grid, bi-linearly for the scalars, and using the method of Akima (1970) for the vector fields (currents). The latter method is based on a piecewise function with slopes at the junction points determined locally by a set of polynomials and known to provide a very accurate solution.

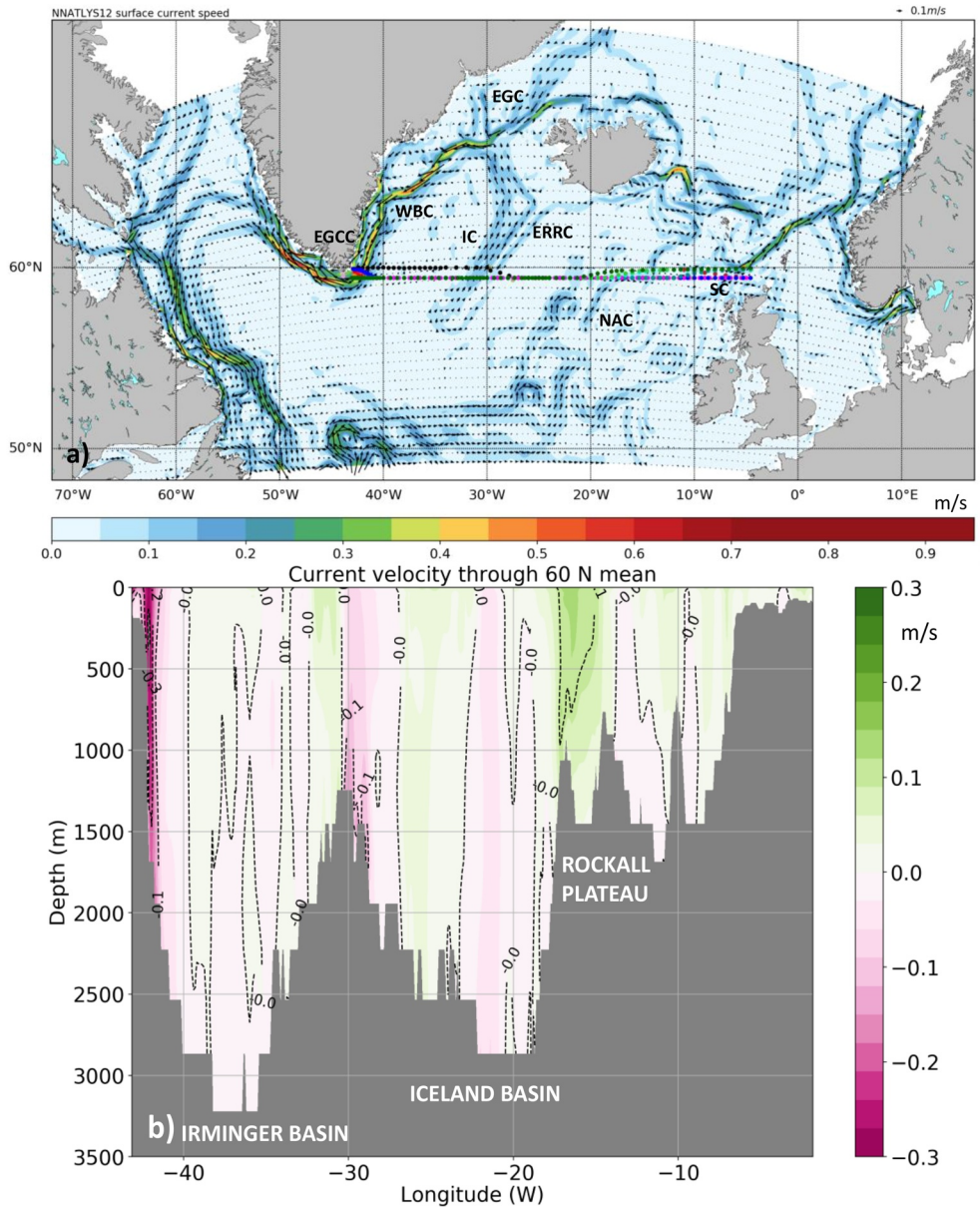

Figure 1. (a) Mean surface velocity for the summer period of 2002–2015 provided by GLORYS12 reanalysis (color shading in m·s^{-1} and vectors) and the location of the 59.5°N section points. (b) Variations with the depth of the mean current (summer period) across the 59.5°N section (positive/negative values indicate northward/southward flows in m·s^{-1}).

3.2. Assessment Method

The assessment of the reanalysis starts from the comparison of T and S to the in-situ measurements at the 59.5°N section. The 2D (depth-longitude) mean fields along the 59.5°N section and the *rms* of their differences are used to quantify the consistency of the reanalysis with the observed fields and to identify the major biases. With a time record short of only 14 samples collected in the summer of 2D T and S fields, statistical analyses have to be used with caution. Nevertheless, we computed the linear trends over these summer records with the least squares and estimated their statistical significance at a 95% level using the squared r-value test.

To assess how the GLORYS12 reanalysis and the two other products, ARMOR and ISAS represent the ocean characteristics along the section, we calculate the time-correlation between the temperature anomalies of

the analyzed datasets and those of the observations over the 14 summers at every hydrographic station and compare their respective distributions. Anomalies were calculated by removing the 14-summer mean and detrended.

The calculation of the ocean heat content at the 59.5°N section is performed for every section using the potential temperature interpolated on the model grid. The temperature at each grid point is first weighted by the volume of the corresponding model grid-cell, and all temperature points are then summed up across the section and over the levels corresponding to the depth ranges 0–700 m and 700–2,000 m.

The analysis of the meridional volume and heat transports based on the observations is limited by the availability of the LADCP data that are crucial for computation. Thus, computations using OBS were performed for the years 2010, 2014, 2015. First, the geostrophic velocities along the section are calculated using CTD data. The velocity data from two upward and downward-looking 300 kHz LADCPs are then used to quantify the barotropic component of the absolute velocities, which are used for volume transport estimation (Visbeck, 2002). Double precision of LADCP velocity estimation is gained using two instruments' data on the way down and up, with the velocity error estimated around 0.03 m/s, which is proven to be a qualitative result according to Thurnherr (2010). The cumulative volume transport accumulated from west to east along the 59.5°N section was derived with 10 km resolution for each of the three sections. For the reanalysis and the two other analyses, cumulative transport was computed for every individual year of the 14-year period (see Appendix).

An accurate assessment of the MHT was not possible for OBS as only the barotropic volume transports and not current velocity profiles were available for this study. Therefore, we use a proxy of the MHT, calculated from the vertically averaged velocity (derived from the barotropic transport from OBS) instead of the full vertical velocity profiles (see Appendix). For GLORYS12 and ARMOR, the MHT is calculated in the same way for comparability. We estimated the error induced by this approximation with the reanalysis data and found that it was always less than a few percent.

4. Results

4.1. Time Mean Characteristics

The long-term mean (2002–2015) surface summer (JJAS) circulation revealed by GLORYS12 (Figure 1a) is in good agreement with the circulation schemes proposed by Daniault et al. (2016) or García-Ibáñez et al. (2015). The six major flow streams crossing the 59.5°N section are the East Greenland Coastal Current (EGCC); the East Greenland Current (EGC), and the southward flowing branch of the Irminger Current (IC) (those three currents forming the Western Boundary Current (WBC) system of the Irminger Basin); the main branch of the IC flowing northward along the western flank of the Reykjanes Ridge; the southward East Reykjanes Ridge Current (ERRC) east of the ridge; and the North Atlantic Current (NAC) flowing northward along the western flank of the Rockall Plateau. We also notice a strong slope (SC) current along the shelf break of the British Isles. Figure 1b shows the mean vertical section of the time-mean meridional velocities across the 59.5°N, the pattern and intensity of which are consistent with the observed current structure shown in Sarafanov et al. (2012) for the 2002–2008 period, except for the deep Irminger Basin where observations report higher (southward) velocities (up to -0.1 m s^{-1}), a feature related to the overflows from the Nordic Seas missed by the reanalysis.

The mean thermohaline structure of the ocean along the 59.5°N section revealed by the observations is well represented by the reanalysis except for the near bottom structure (Figures 2a, 2b, 2d and 2e). Differences in the mean fields are in the range of ±0.1°C for temperature and ±0.01 for salinity over a large part of the section. The *RMS* values of the differences (*RMSD* hereafter, Figures 2c and 2f) are small in the regions where stratification is weak (Brunt-Vaisala frequency $N < 2 \times 10^{-5}\ s^{-1}$), for example, below the summer (main) thermocline in the Irminger (Iceland) basin, and between 100 and 800 m in the region of the Rockall Plateau. The largest values of the *RMSD* (~0.8°C for T and ~0.07°C for S) are observed in the well-stratified layers ($N > 2 \times 10^{-5}\ s^{-1}$) captured by 5°C and 8°C isotherms in Figure 2a, and in the boundary currents that flow along the continental slope of Greenland and the eastern flank of the Reykjanes Ridge. In the main thermocline, the pattern of the *RMSD* holds the imprint of vertically coherent mesoscale structures. It cannot be ruled out that these structures are spurious values introduced in the temperature

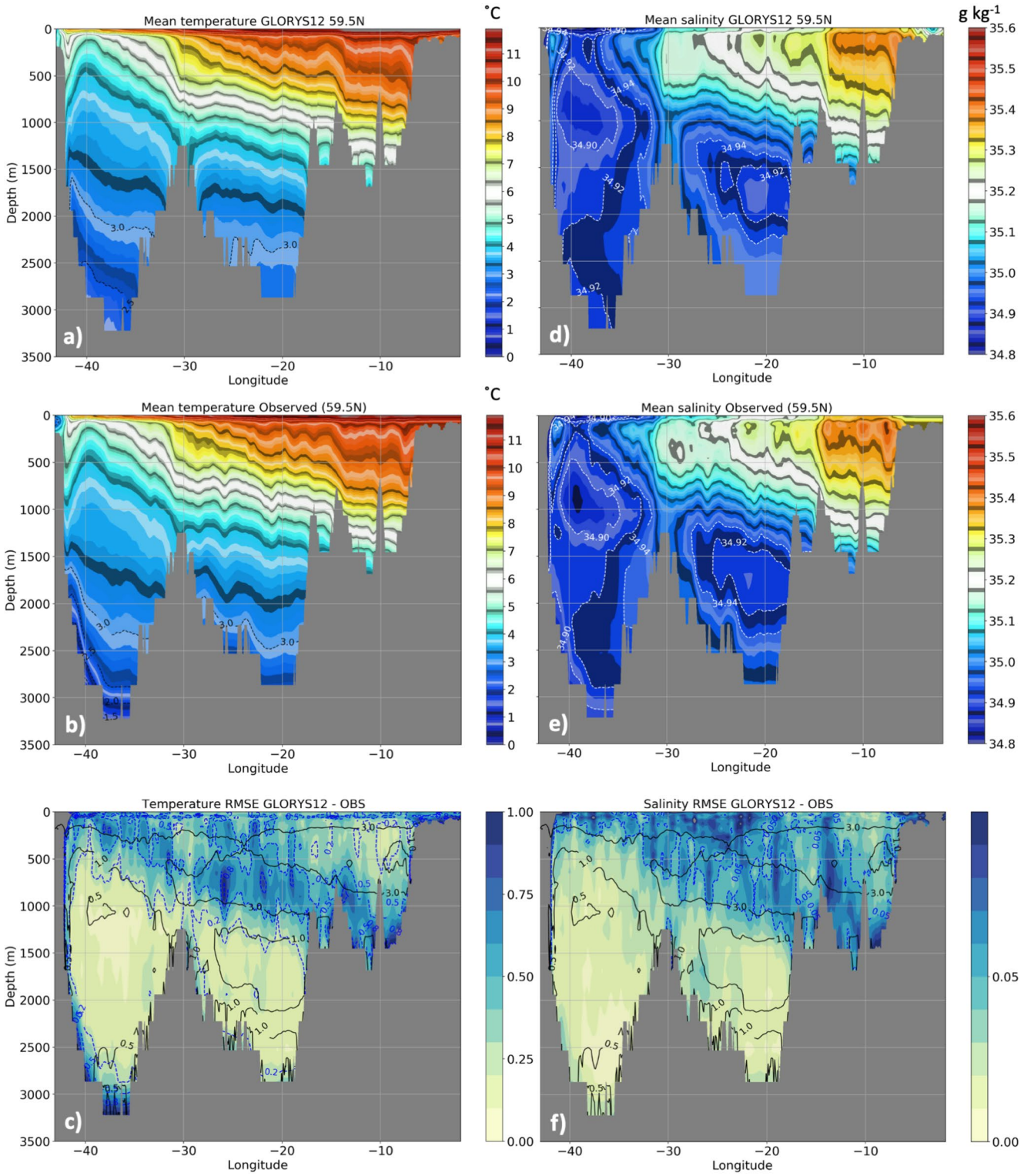

Figure 2. Mean (period of 2002–2015) potential temperature (°C), and salinity along the 59.5°N section for (a),(d) GLORYS12 (b),(e) OBS, and (c),(f) the root mean square of the differences (*RMSD*) between the two datasets (colors). Dotted lines in (c),(f) are isolines of the Brunt-Vaisala frequency (in 10^{-5} s^{-1}).

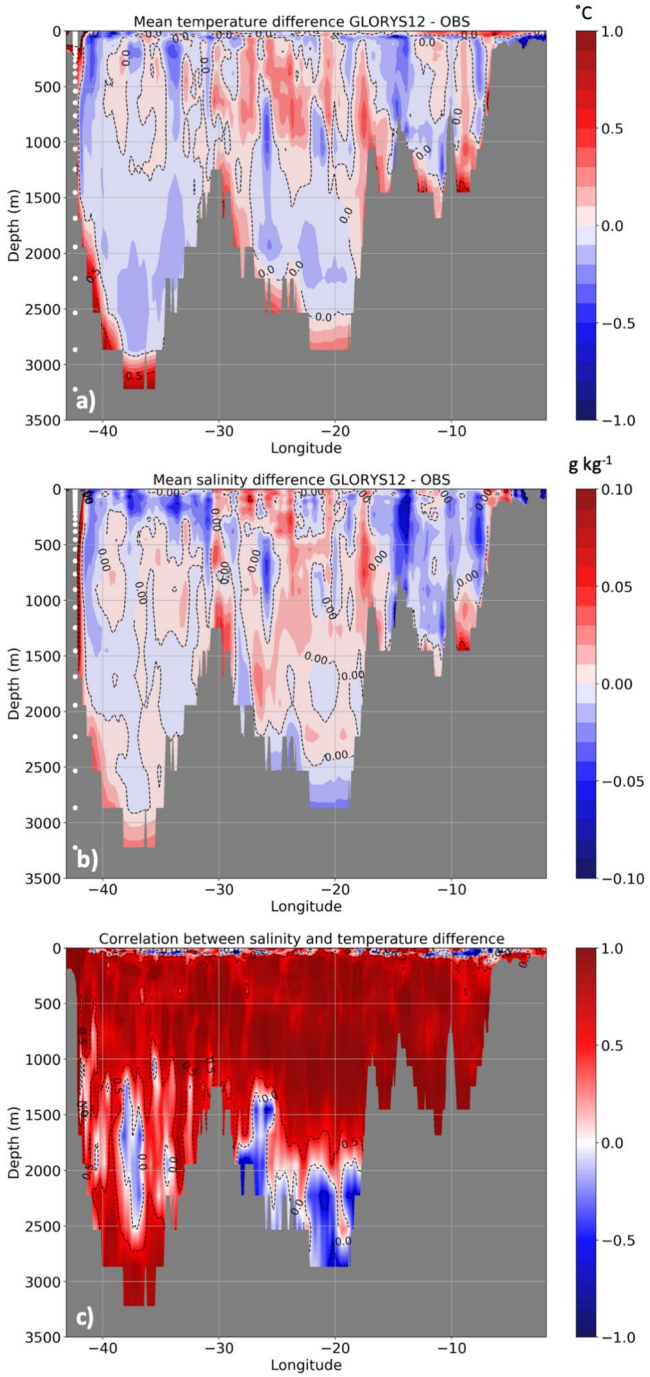

Figure 3. Differences in mean (period 2002–2015) (a) Temperature and (b) Salinity between GLORYS12 and observational data set (OBS), and (c) time-correlation (over 14 samples) between the *T* and *S* differences (see Appendix for this calculation). Positive (negative) correlations indicate that warmer/cooler waters are also saltier/fresher (fresher/saltier). White dots along the depth axis in panels (a) and (b) indicate the model vertical levels.

profiles by inconsistencies in the multivariate assimilation of the altimetry signal (that only partly accounts for the mesoscale). Nevertheless, it is also likely that they result from the mismatch in the instantaneous positioning of mesoscale circulation features (current meanders, eddies, and fronts) rather than from systematic *T, S* biases. Although the reanalysis assimilates the along-track altimetry data, which should allow for capturing these features, small mismatches in positioning or amplitude of mesoscale structures do exist, being especially evident in the regions of large gradients.

Figures 2a–2d shows that the T/S fronts over the Rockall Plateau have a similar position in the reanalysis and in OBS. This location is also where the RMSE in salinity is large (Figure 2f) and corresponds to the location of the NAC in Sarafanov et al. (2012) (their Figure 4c). Since the front is highly variable, this region is also the place where year-to-year differences in salinity between the two datasets are the greatest, despite very comparable mean values. This location is also where we observe a large positive trend in S in both datasets (Figure 4).

Large values are also found in a very thin layer near the depth of 45 m, where the reanalysis is systematically cooler and fresher (it is quite obvious in Figure 3c). It is difficult to understand the sources of the biases as many different factors can contribute. The fact that the T and S differences are anti-correlated (they do not compensate in density, Figure 3c) suggests a problem in the multivariate assimilation algorithm of SST that may generate spurious salinity values near the bottom of the shallow summer thermocline. Indeed, incoherencies between the temperature and salinity increments calculated by the atmospheric forcing (i.e., the output of the bulk formulas) and the assimilated SST data provided by an analysis of satellite observations are very likely to exist that the assimilation algorithm has difficulty in removing.

The large values of the *RMSD* along the Greenland shelf break and from 1,500 m down to the bottom in the Irminger Basin, and at the eastern flank of the Reykjanes Ridge below 1,200 m (Figures 2c and 2f), demonstrate that the reanalysis fails to adequately reproduce the properties of the overflows from the Nordic Seas. The overflow waters are significantly warmer (by 0.5°C–1°C) and saltier (by 0.03–0.05) in the reanalysis compared to the observations (Figure 3). The reanalysis is not directly constrained by observations collected at these depths (the Argo array does not cover the ocean below 2,000 m). Those biases in the overflow properties indicate that the present assimilation system is not able to improve the poor representation of the Denmark Strait overflow by the ORCA12 numerical model (Colombo et al., 2020).

Differences in mean temperature between GLORYS12 and OBS demonstrate that the reanalysis is warmer over ~65% of the section, mainly in the highly stratified layers, and is cooler in the layers where stratification is weak (Figure 3a). The reanalysis is also saltier over ~64% of the section (Figure 3b). The pattern of the differences between the reanalysis and OBS in temperature and salinity is remarkably consistent with each other over most of the domain (correlation > 0.9 for 90% of the points), with warmer waters being also saltier (Figure 3c), thus partly compensating their respective contributions to the density field. However, some noticeable exceptions (negative correlations often beyond −0.5) are observed in the deep Iceland basin (from 1,800 m down to the bottom), in the core of the low stratified waters in the central Irminger basin (between 1,200 and 2,500 m–this is the LSW

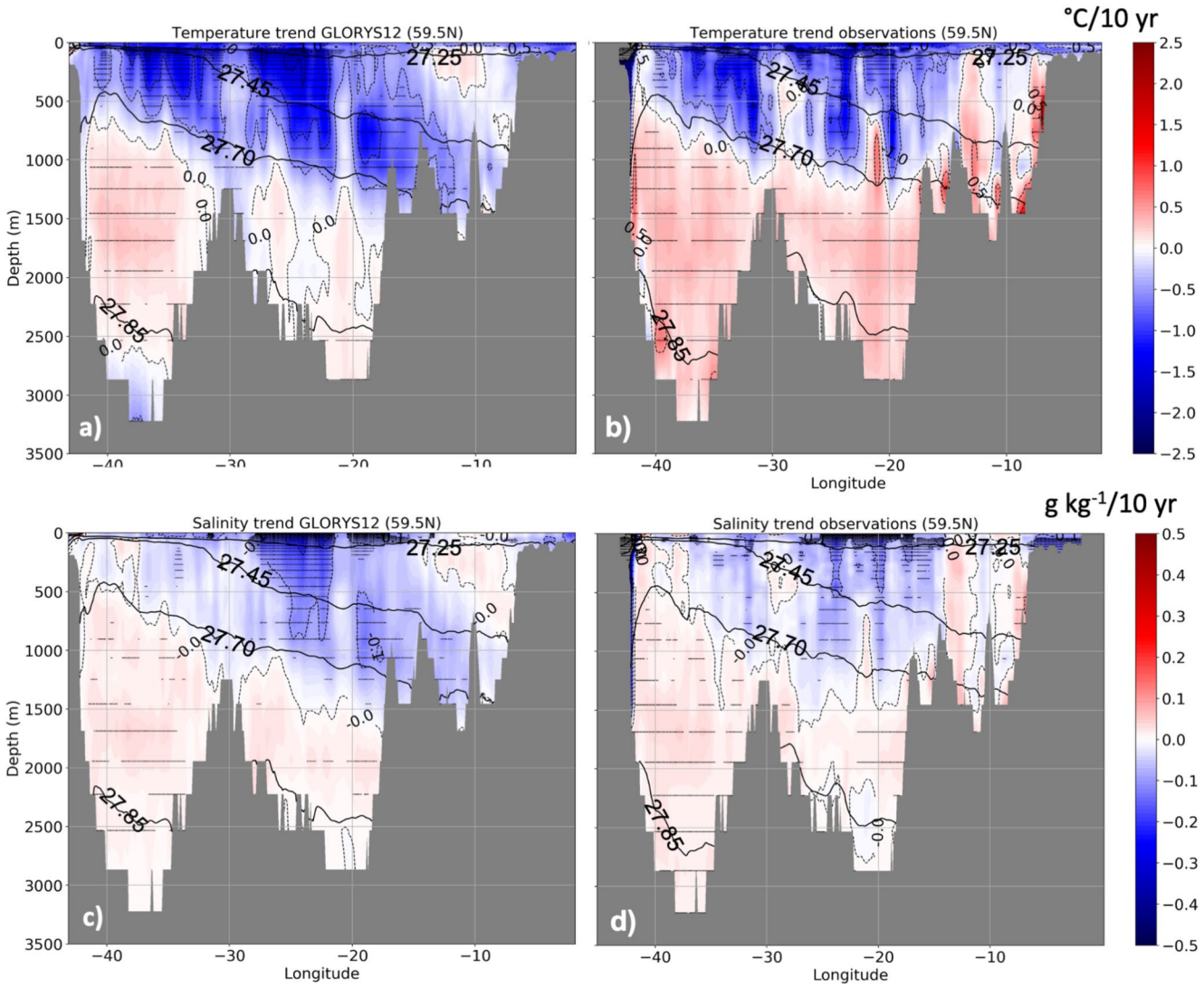

Figure 4. Linear trends over the 14 years period (2002–2015) in potential temperature (top panels, in °C per decade) and salinity (bottom panels, in g·kg^{-1} per decade) as represented by the observations (right panels) and the reanalysis (left panels) along the 59.5°N section. Horizontal gray lines depict points with a 95% level of trend significance. Thin dotted contour intervals are 0.5°C for temperature and 0.1 g·kg^{-1} for salinity. Bold black contours indicate the 27.25, 27.45, 27.65, and 27.85 isopycnals (σ_0).

layer), and in the mentioned already very thin layer below the surface. These warmer (cooler) waters are also fresher (saltier) compared to OBS, thus suggesting changes in the density field.

4.2. Interannual Variability

We now turn to the assessment of representation of the ocean variability in the reanalysis. Figure 4 examines the linear trends in GLORYS12 and in the observations at 59.5°N over the period 2002–2015. We use linear trends here as an effective metric for the comparative assessment rather than for assessing ocean state climate tendencies, which can hardly be evaluated from a rather short 14-yr record of the hydrographic data. The dipole-like trend pattern in T and S seen in the observations is qualitatively well captured by the reanalysis, with a cooling (at maximum being −1.5°C per decade) and freshening (salinity trend of −0.1 per decade) within and above the thermocline ($\sigma_0 < 27.70$), and warming of about +0.3°C per decade and salinification of 0.02–0.04 g·kg^{-1} per decade in the deep ocean.

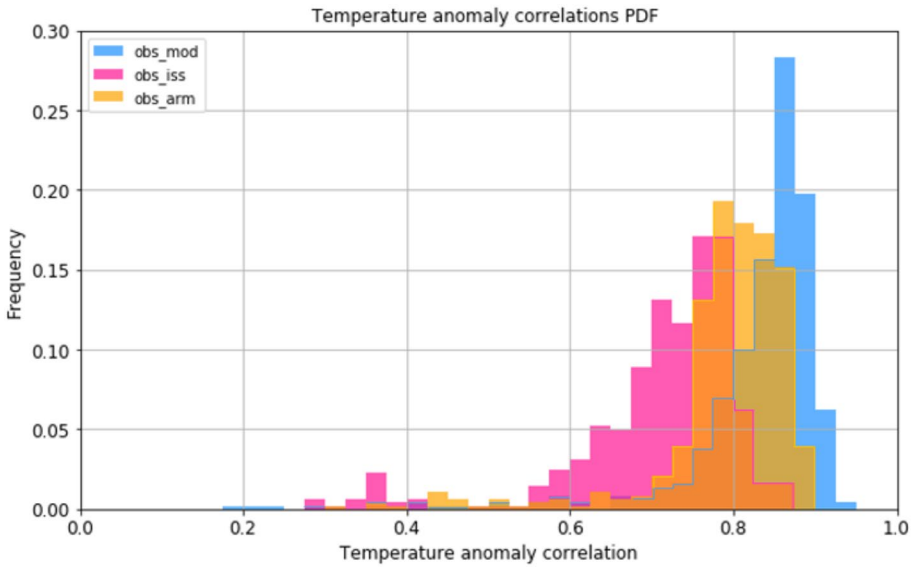

Figure 5. Distribution of the correlation coefficient values describing how the temperature variations of a given data set (GLORYS12 in blue, ARMOR in yellow, and ISAS in red) are correlated in time with those of observational data set (OBS) at every point of the section array of the 59.5°N section.

The positive temperature trends are somewhat weaker in the reanalysis and exhibit alternation of slightly positive and negative trends below 1,500 meters in the Iceland Basin, where observations show a robust pattern of positive trends (Figure 4a). These differences in the trend magnitudes lack, however, statistical significance. Observations also show locally strong but insignificant trends along the topographic features of the Rockall Plateau and the Scottish shelf break, which are not detectable in the reanalysis. In turn, the reanalysis exhibits locally strong negative (but also statistically insignificant) trends in the near–bottom layer of the Irminger Basin, while the observations report statistically significant positive trends.

The agreement between trend estimates in reanalysis and observations is closer for the salinity than for the temperature (Figures 4c and 4d). Trend magnitudes are quite close to each other except for the upper layer of the Iceland Basin, where the reanalysis exhibits stronger trends. Discrepancies were also found over the Rockall Plateau, where the reanalysis and observations show trends of the opposite sign, while both are statistically insignificant.

We now attempt to quantify the value added by the dynamical interpolation (i.e., based on a predictive physical model) performed by GLORYS12 in comparison to ARMOR and ISAS diagnostic interpolation (based on a physical diagnostic model). We calculated at every depth-longitude point of the common grid the time correlation of the detrended anomalies of the temperature of the observational data set (OBS) with those of GLORYS12, ARMOR, and ISAS. For each of these datasets, we obtain a set of correlation coefficients quantifying how well the data set is correlated in time with the observations at every point of the section array. The distribution of the correlation coefficients is displayed in Figure 5. It reveals that the ISAS statistical analysis, which is monthly and does not use altimetry and is less capable of representing the variability seen in the in-situ observations compared to the ARMOR statistical analysis, which includes the altimetry. Figure 5 also demonstrates that the model-based dynamical interpolation of GLORYS12 performs (in terms of variability) better than the ARMOR statistical analysis, although both use equivalent datasets to constrain the analysis. Therefore, GLORYS12 appears to be the most accurate data set among the three analyses in representing the characteristics and variability of the ocean along that section.

4.3. Heat Content and Meridional Transports

Ocean heat content (OHC) and meridional heat transport (MHT) represent key climate indicators, and their variability is critically important for assessing changes in the ocean state and dynamics (Meyssignac et al, 2019; von Schukmann et al., 2016a, 2016b). Thus, representation of OHC and MHT in ORAs is of high

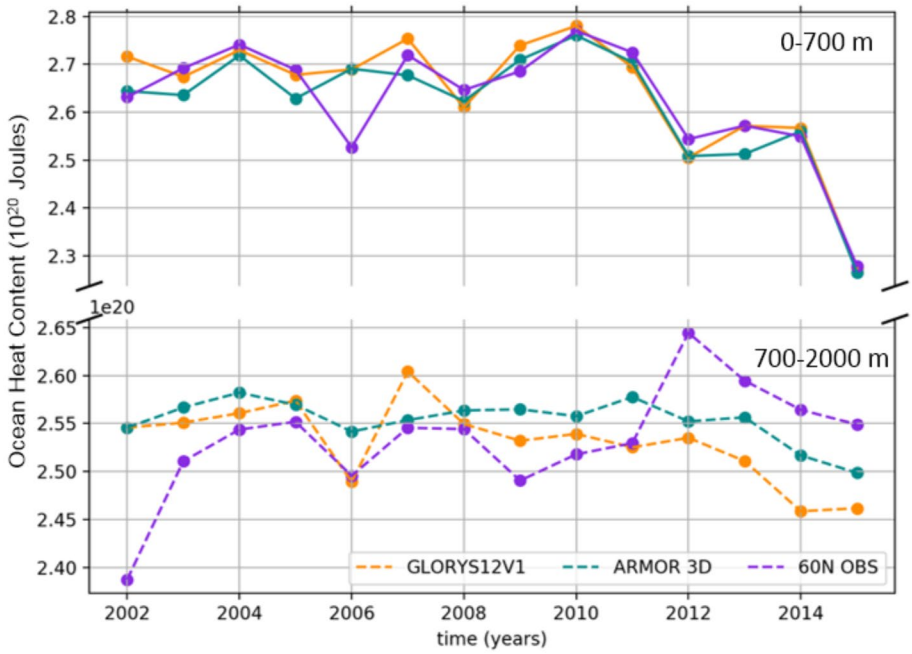

Figure 6. Evolution of the total ocean heat content at the 59.5°N section in the depth range 0–700 m (upper panel) and in the depth range 700–2,000 m (lower panel).

priority, as most present estimates implying the impact of ocean heat accumulation on the global heat storage change are based on the analyzed products (e.g., Balmaseda et al., 2013 among others).

The OHC at the 59.5°N section has been calculated for the depth ranges 0–700 m and 700–2,000 m from the in-situ observations OBS, GLORYS12, and ARMOR products (Figure 6). All three estimates are quite consistent with each other in the depth range 0–700 m (correlations of OBS with ARMOR and GLORYS12 being 0.90 and 0.91). An exception is observed in 2006 when a minimum in OHC is seen in the observations and not reported by ARMOR and GLORYS12. The SODA3.4.2 reanalysis (0.25°) also does not capture this feature and shows, in general, a smaller negative trend in OHC (from the personal discussion with Jim Carton). All three datasets agree on a strong decrease in OHC from 2014 to 2015, likely related to the 2015 cold anomaly in the subpolar gyre reported by Josey et al. (2018) during winters 2013–2016.

The consistency between the three datasets in the layer 700–2,000 m is, however, worse compared to the upper ocean layer. The two analyses show larger OHC than that OBS over the period from 2002 to 2011. Also, GLORYS12 and OBS consistently agree on a smaller OHC in 2006 marginally represented in ARMOR. However, both GLORYS12 and ARMOR do not capture the large OHC increase seen in the observations in 2012. As a result, the biases of $\sim 0.05 \times 10^{20}$ and $\sim 0.1 \times 10^{20}$ Joules (for ARMOR and GLORYS12 respectively) persists in the records (Figure 6) after 2012, while all three datasets agree on a continuous decrease of OHC from 2012 to the end of the period.

The full depth cumulative MVT (meridional volume transport, from west to east) across 59.5°N is shown in Figure 7a for the three products (GLORYS12, OBS, and AMOR) for the three chosen years with LADCP observations (2010, 2014, and 2015). The transports by the western boundary current system (from 41°W to 37°W, thus including part of the Irminger Gyre) and by the interior flow (39°W–5°W) are plotted separately in order to eliminate the shift caused by the differences in the WBC magnitude in the different products on the rest of the section.

Year-to-year variations in WBC transport are not consistent across the different products (Figure 7a, left panel). Strong variability in the WBC in OBS (up to ~20 Sv difference from year to year) is consistent with the interannual variability at a similar location of the OVIDE section (Daniault et al., 2016). Note that the OVIDE estimate for 2010 is ~35 Sv, and it is ~48 Sv in OBS at 60°N, although both sections were carried out in summer. Year-to-year variability is much smaller in GLORYS12, but the time mean WBC transport

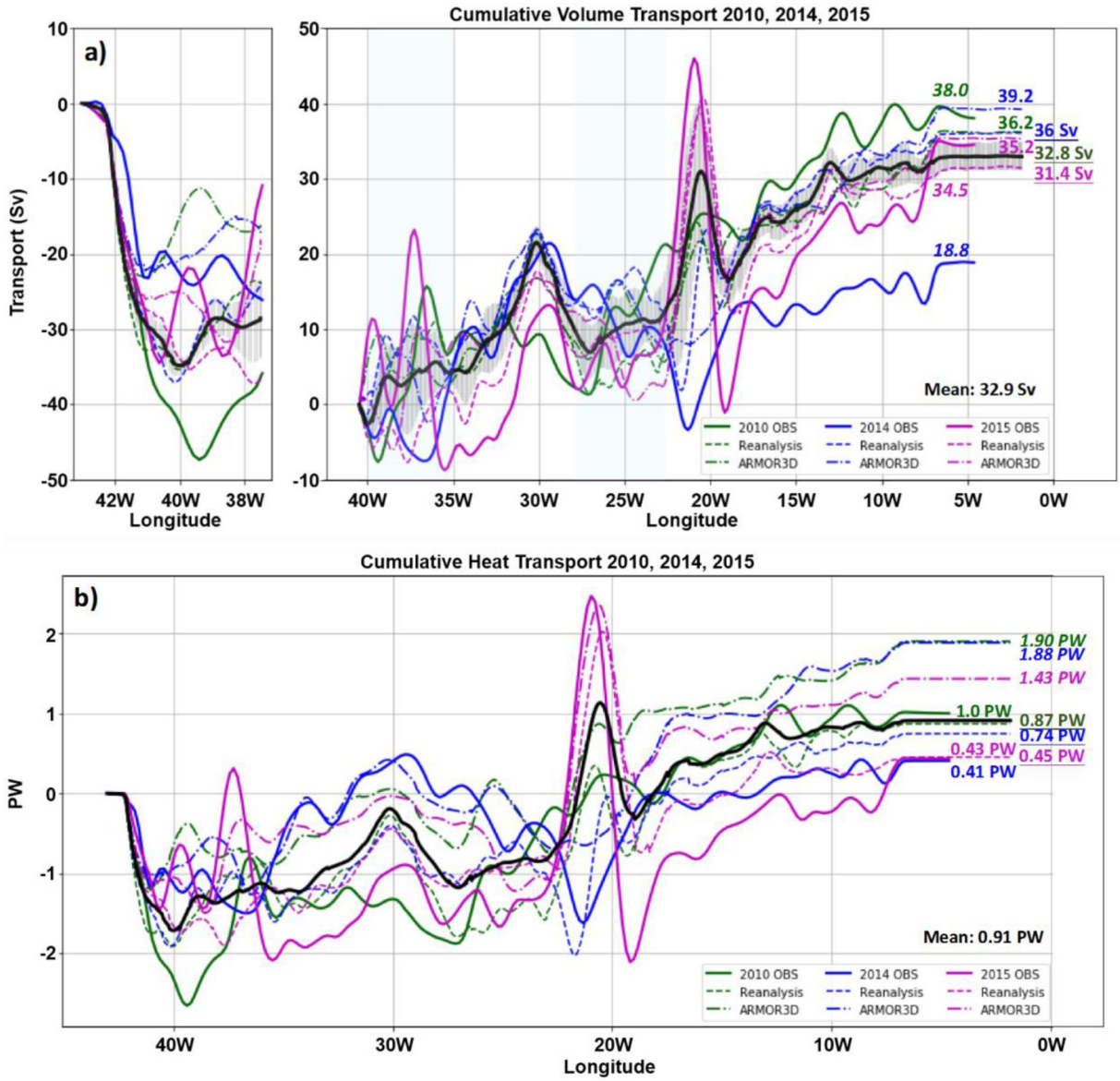

Figure 7. Eastward accumulated meridional (a) volume (separated between western boundary current and interior flow), and (b) heat transport along the 59.5°N section starting from Greenland, for years 2010 (green lines), 2014 (blue lines), and 2015 (purple lines) for the Observations, GLORYS12, and ARMOR3D (see legend). The thick black line represents the 2002–2015 mean cumulative meridional volume transport (MVT) and meridional heat transport (MHT) of the reanalysis. The gray shading in (a) shows the standard deviation of the volume transport in GLORYS12 calculated with all sections (2002–2015).

(32.5 Sv) is in good agreement with the independent estimates (~33 Sv) by Våge et al. (2011) and Daniault et al. (2016). Of the three datasets analyzed, ARMOR always exhibits the lowest WBC transport.

In the interior flow (Figure 7a), the variability of the MVT is again greater in OBS than in the GLORYS12 and ARMOR. Reanalysis shows large STD values (10–15 Sv) in the deep parts of the Irminger (40°W–35°W) and Iceland (28°W–23°W) Basins. In these domains (blue shading in Figure 7a), the structure of MVT is characterized by mesoscale variability imposing the pattern which differs from year to year, resulting in disagreement between datasets, even between GLORYS12 and ARMOR, which both use altimetry. This suggests that mesoscale variability dominates here and that the analyses do not properly catch the impact of these eddies in this area, possibly due to a lack of resolution in the AVISO along-track altimetry signal at this latitude.

In the other parts of the section, estimates of MVT from the analyzed datasets qualitatively compare well with those derived from OBS (with a better agreement for GLORYS12 than for ARMOR) except for a few striking events. In 2010, there is no clear evidence in OBS of the Irminger Current (northward) at the west side of Reykjanes Ridge (33°W–30°W), possibly because of the presence of an intense anticyclonic eddy adjacent to the IC, whereas the IC is well identified in GLORYS12 and ARMOR.

Also, a special analysis is needed to understand the very large variability seen in the MVT in the main branch of the NAC (23°W–19°W), where GLORYS12 shows the greatest STD values (~20 Sv). In 2015, in OBS, this feature is characterized by an intense northward transport (36 Sv) between 23°W and 21°W, a very strong southward recirculation (−47 Sv) between 21°W–19°W, and a northward recovery between 19°W and 17°W of a lesser amplitude (17 Sv). Both GLORYS12 and ARMOR demonstrate the same pattern in 2015 with a slight eastward shift of the current reversal and lesser strength of the reversal. The pattern for 2014 is alternatively characterized by an intense southward flow (13 Sv) between 23°W and 21.5°W and a strong return flow (17 Sv) at 21.5–18°W. Again, both GLORYS12 and ARMOR in 2014 demonstrate similar patterns. In 2014 the transport of this branch of the NAC flowing on the western part of the Rockall Plateau (~18°W–13°W) is particularly weak in OBS (being about 10 Sv or more in the other datasets). This weakness leads to anomalously low total cumulative transport for the interior flow (18.8 Sv), which is significantly smaller than the 30–40 Sv seen in other years and analyzed products. None of those patterns is seen in 2010 in any other data set. In the next subsection, we verify the hypothesis that these patterns are due to particularly large and intense anticyclonic or cyclonic eddies that were well captured by the altimetry and thus reproduced in the analyses, especially in GLORYS12.

In the reanalysis, the 14-yr mean transport (black curve in Figure 7a) resembles the pattern seen in the observations in 2015 (full purple line), suggesting that this situation is predominant in the reanalysis. Indeed, this pattern is found eight times in the 14-year record of GLORYS12. We found that the pattern observed in 2014 (a very weak MVT at 21.5°W, full blue line) occurred four times in the record, that there were 2 years of the record when none of these patterns were clearly detected.

The cumulative MHT (Figure 7b) does not separate the contribution of the WBC from that of the interior flow. It is calculated with the barotropic velocity (see Appendix) and follows in principle the MVT. Thus, the discussion about the inconsistencies of MVT is also applicable to findings related to MHT. The year-to-year spread of the estimates of MHT is large in all three datasets, with the largest variability being in OBS. There is no agreement between estimates of MHT in the boundary current and in the central parts of the Irminger and Iceland basins where mesoscale eddies determine the flow. A better agreement is found in the other parts of the section. Considering the MHT across the whole section, it appears to be too high in ARMOR exceeding other estimates by ~1 PW. This shift can be partly explained by the weak MHT in the boundary current (0.6 PW), illustrated in Figure 7b, by the strong difference seen between any of the ARMOR MHTs and the 14-yr mean MHT of GLORYS12 at 37.5°W. An additional 0.4 PW of the difference is mainly due to the representation in this analysis of the southward flow associated with the large eddy-like pattern at 22°W–20°W, which is smaller than in the other datasets.

The agreement is rather good between GLORYS12 and the observational estimates in 2010 (0.87 PW and 1.0 PW respectively) and in 2015 (0.45 PW and 0.43 PW, respectively). The difference in the total MHT seen between GLORYS12 and OBS in 2010 (0.74 PW and 0.41 PW, respectively) should be likely related to the weak transport in the NAC on the western side of the Rockall Plateau, as was mentioned previously.

4.4. MVT Analysis for 2014 and 2015

The ORCA12 circulation model has a grid resolution of 4.625 km at 60°N. Such resolution, which only marginally resolves the eddy scale (the Rossby deformation radius being between 8 and 12 km in this region, Chelton et al., [1998]), allows for the generation of mesoscale circulation features such as current meanders, fronts, coherent eddies, as illustrated in Figure 8a, but their characteristics do not compare well with the observed one. The assimilated along-track sea level anomalies have a resolution of 1/3°, which is insufficient to represent the mesoscale at this latitude accurately but could help in positioning the eddies of the greatest amplitude. Therefore, we cannot expect the GLORYS12 reanalysis system to resolve eddies (i.e., it accurately represents the mesoscale eddy field, its generating instability processes, and its effects on the state of the

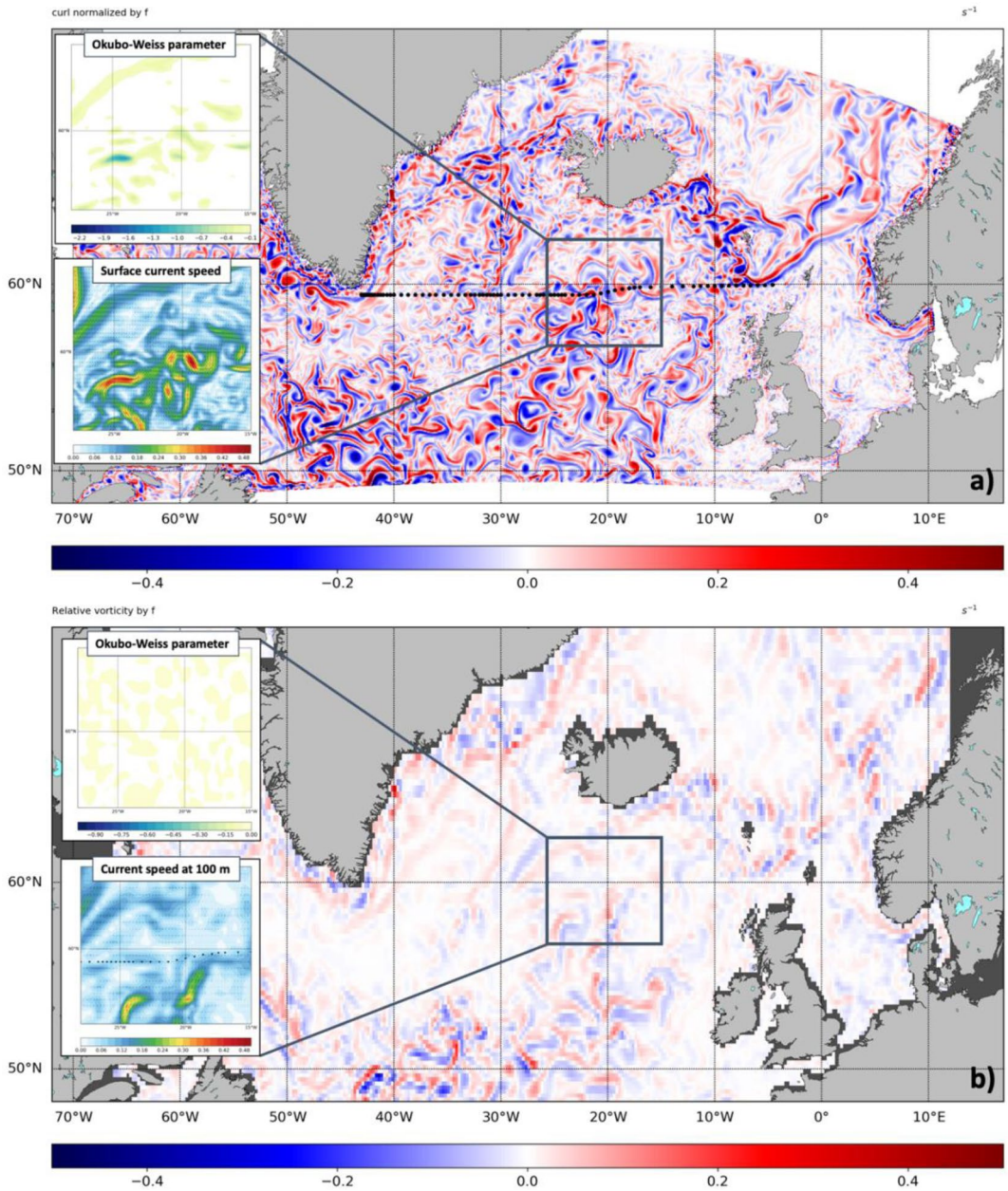

Figure 8. Snapshot (on 16/06/2015) of the relative vorticity normalized by the Coriolis parameter as provided (a) by a free run (NEMO code, no assimilation of observations) at 1/12° resolution, (b) by the medium resolution (1/4°) reanalysis GLORYS025. Insets show respectively the Okubo-Weiss parameter and the current speed and direction in the domain delimited by the gray box. The corresponding figure for the 1/12° GLORYS12 reanalysis is shown in Figure 10c.

ocean). Nevertheless, the eddy field of GLORYS12 (Figure 10c) compares very well with that of the ORCA12 free run (Figure 8a), which indicates that the reanalysis system does not hamper the ability of the dynamical model to generate eddies. The comparison with the lower resolution reanalysis GLORYS025 (Figure 8b) demonstrates that the increase of resolution from 1/4° to 1/12° brings dynamically consistent (i.e., consistent with the dynamics resolved by the model) information on the mesoscale eddy field. Therefore, the eddy field of the reanalysis may be used to understand specific circulation features seen in the observations.

The Okubo-Weiss parameter often used to track coherent mesoscale eddies (D'Addezio et al., 2020; Vortmeyer-Kley et al., 2016) allows separating the vorticity-dominated and deformation-dominated flow areas.

It is used in eddy activity analysis to distinguish the coherent eddying structures from ones with intense shear.

4.4.1. MVT in Summer 2014

The maximum cumulative MVT at 30°W (∼20 Sv) is a common feature of all products (Figure 9a). It results from a complex pattern of the IC on the western flank of the Reykjanes Ridge. The temperature front reaching the depth of 800 m on this slope (Figure 9b) indicates that the northward predominantly barotropic flow determines the transport, which is confirmed by the vertical current profiles (see Supplementary Figure S2 for that date, it is also well-identified in the mean current shown in Figure 1b). However, mesoscale disturbances in the temperature front suggest the presence of meanders or eddies in the current, confirmed by the presence of thin surface or bottom intensified southward jets (Supplementary Figure S2). The relative vorticity (and the map of the Okubo-Weiss parameter, not shown) confirms the dominance of large meanders in the Irminger Current and a few coherent eddies (Figure 9c) rather than a continuous current as is the case for example for the East Greenland Current. Another essential feature of the MVT is the mesoscale pattern between 23°W and 20°W characterized by an MVT minimum at ∼23°W (detectable in all datasets except ARMOR, and weaker in GLORYS025, Figure 9a) and associated with a strong southward flow. In this longitudinal band, the relative vorticity field (Figure 9c) shows cores of cyclonic and anticyclonic vorticity, the amplitude of which is significantly greater than the background, as shown by the large values of the Okubo-Weiss parameter (inlet in Figure 8c). This latter parameter suggests the presence of a coherent cyclonic eddy which is confirmed by the surface velocity (inlet in Figure 9c), which locates its center at 21.5°W, in agreement with the vertical temperature structure in this part of the section (Figure 9b).

4.4.2. MVT in Summer 2015

In summer 2015, a large MVT was visible between 22°W and 18°W (Figure 10a) in all datasets except in the 1/4° resolution reanalysis, which misses this pattern (likely because the resolution is too coarse to produce or maintain eddies at this high latitude). Consistently with GLORYS025, SODA3 reanalysis with a similar diagnostic also does not capture this eddy (Jim Carton, *personal communication*). The vorticity field (Figure 10c) shows that the section is passing through a large and intense mushroom-shaped mesoscale pattern with an anticyclonic vortex (22°W–20°W) characterized by a sharp deepening of the isotherms in the part of the section adjacent to a cyclonic vortex (20°W–18°W) marked by a doming of isotherms (Figure 9b). To be sure that this structure can be referred to as "eddy," we provide here the Okubo-Weiss parameter analysis (see Figure 9c), which shows the coherent structure of the anticyclonic eddy. The maps of the Current Velocity and the Okubo-Wiess parameter (inlets in Figure 10c) relate this pattern to the presence of a strong anticyclonic vortex (A) with a core located at 20°W, adjacent to a cyclonic vortex (C) north of it. The large northward transport (∼30 Sv) in the main branch of the NAC between 22°W and 20.5°W (Figure 10a) feeds the intense southeastward flow (∼30 Sv) between the two vortices at 20.5°W–19°W. The mushroom shape of the eddy suggests that the eddy is in a phase of generation from the instability of the NAC (Etling et al., 1993; Fedorov & Ginsburg, 1986; Fedorov et al., 1989; Mied et al., 1991; Simpson & Lynn, 1990). The vortices (as revealed by the vertical temperature structure in Figure 10b and by the vertical profile of the current speed (Supplementary Figure S3) are intensified above 1,500 m, but their signature reaches down to the bottom, implying that the associated flows have a strong barotropic component. Note that the MVT pattern is shifted to the west in GLORYS12 compared to observation (Figure 10a), likely because the anticyclonic eddy is not precisely co-located in space with observations. The imprint of this shift on the T and S fields very likely contributes to the large value in the T and S RMSD shown in Figure 2.

Therefore, the reanalysis allows for a clear association of the eddy-associated features in MVT and MHT derived from the observations. The variability seen in the reanalysis in the branch of the NAC flowing west of the Rockall Plateau (∼20°W) indicates that this region is characterized by the intense generation of large mesoscale eddies, which are potentially well captured by satellite altimetry.

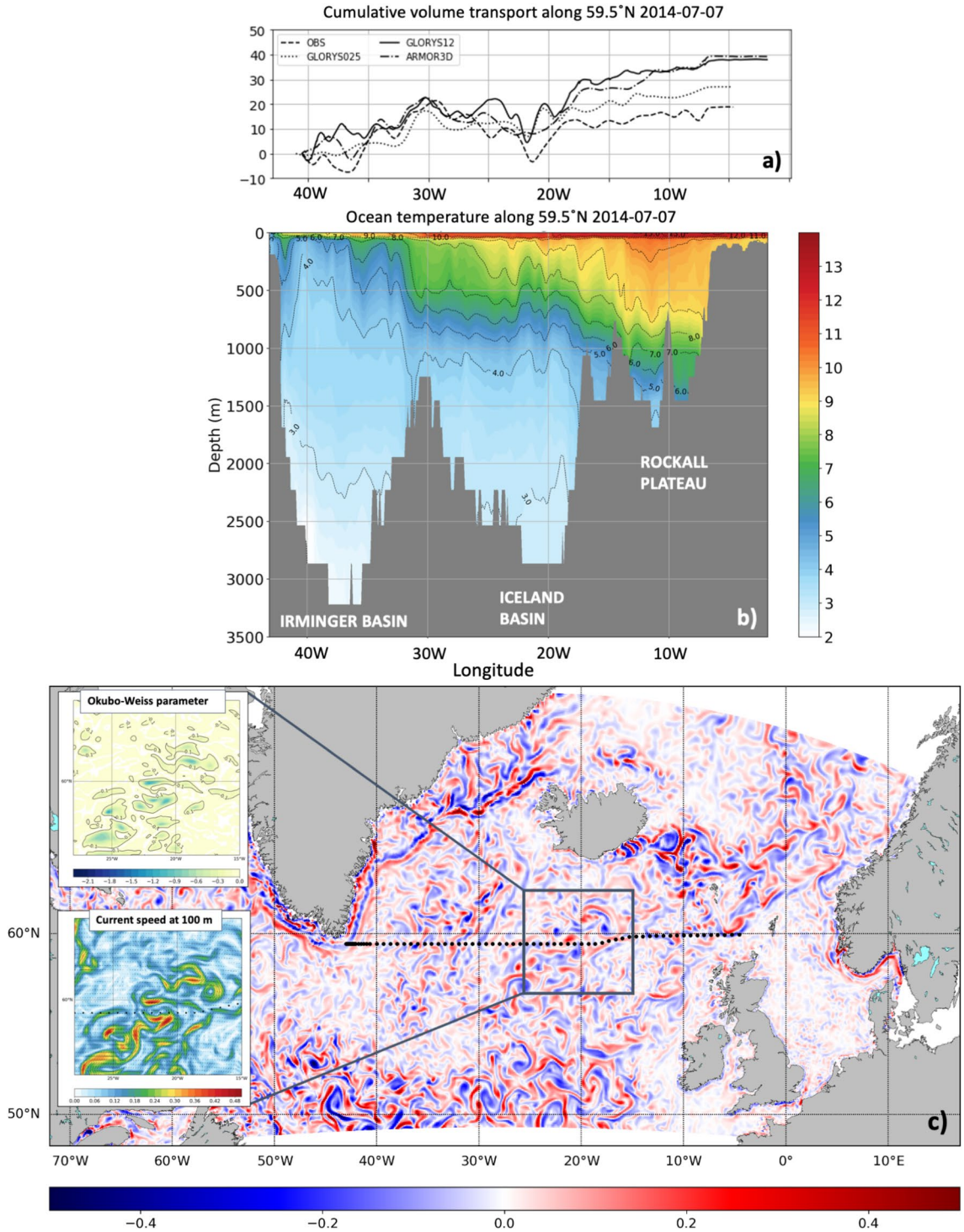

Figure 9. (a) Cumulative volume transport (in Sv) along 59.5°N starting from 40°W for the observations and the various analyzed datasets in summer 2014. Reanalysis transports correspond to the central date of the section deployment (07/07/2014). (b) Vertical distribution of the potential temperature along 59.5°N and (c) the surface relative vorticity normalized by Coriolis parameter in the 1/12° reanalysis (07/07/2014). The Black dotted line in (c) depicts the positions of the hydrographic stations in 2014. The inserts show the Okubo-Weiss parameter and the surface currents in the Iceland Basin.

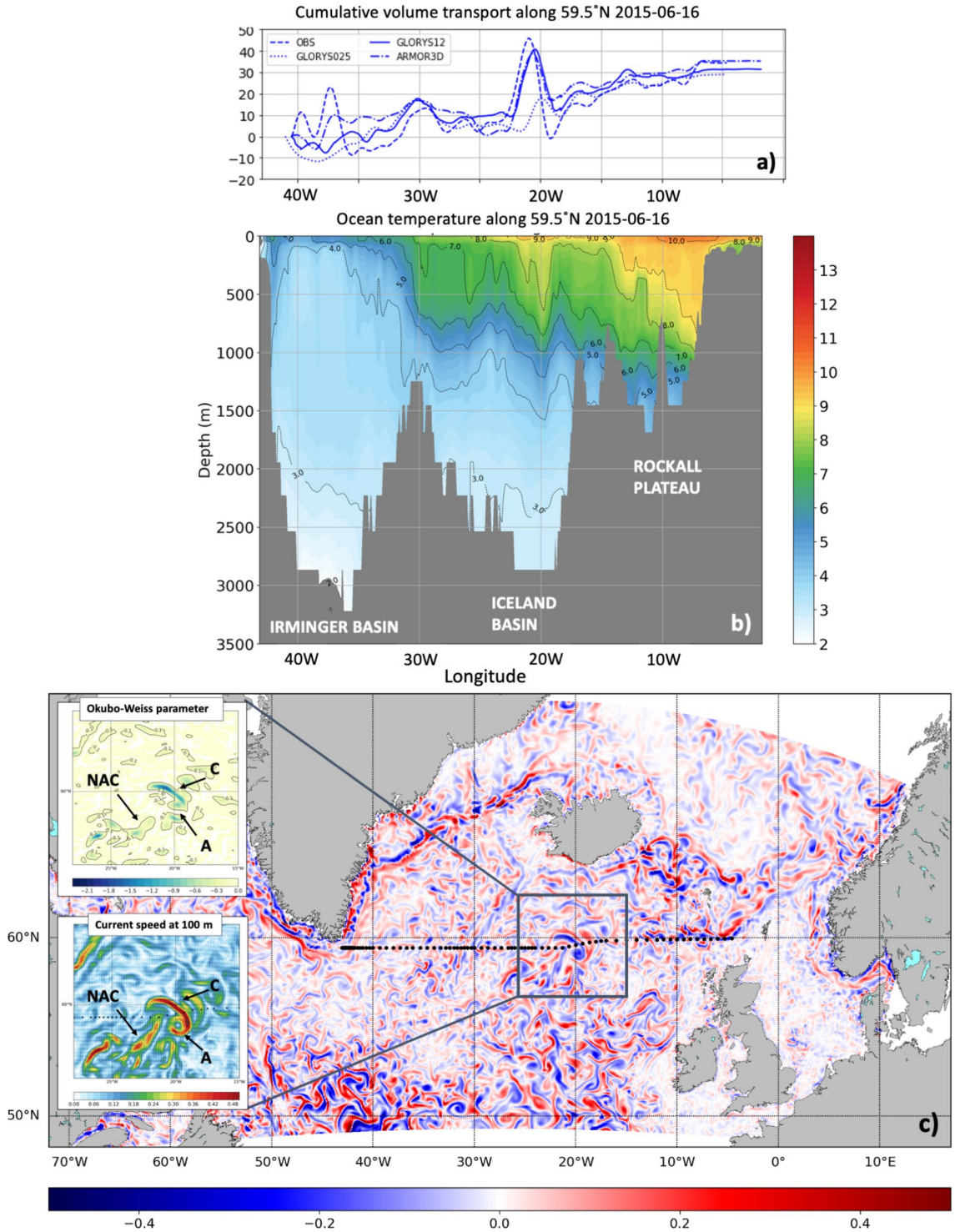

Figure 10. Same as Figure 9 for the date of 16/06/2015. A and C in the inlets refer to the Anticyclonic and the Cyclonic Eddies described in the text, and North Atlantic Current (NAC) refers to the main path of the northern branch of the North Atlantic Current (see Figure 1a).

5. Summary and Conclusion

The first eddy-resolving ocean reanalysis GLORYS12 produced by Mercator Ocean International was validated against 14 years (2002–2015) of independent observations (i.e., not assimilated in the reanalysis system) at the 59.5°N section in the North Atlantic. To provide more comprehensive validation, two blended products, ISAS15 and ARMOR3D, which use the same datasets as GLORYS12, were additionally used.

GLORYS12 reproduces the main circulation pattern of the Subpolar Gyre realistically and also provides a realistic representation of the mean vertical structure of the currents across the 59.5°N section in agreement with the recent observational studies (Daniault et al., 2016, García-Ibáñez et al., 2015; Sarafanov et al., 2012).

The mean thermohaline structure of the ocean at the 59.5°N section revealed by OBS is well represented by GLORYS12 except for the near bottom structure. The agreement in T and S fields, characterized by *RMSD*, is the highest below the main thermocline in the Irminger and Iceland basins, where the stratification is weak. The agreement is, however, weaker within the well stratified main thermocline (between the 5°C and 8°C isotherms). Imprints of vertically coherent mesoscale structures noticed in the thermocline can be attributed to the fact that the instantaneous positioning of mesoscale circulation features are not exactly co-located in the reanalysis and observations. Surprisingly, highly localized large RMSD values are also found at 45 m depth, suggesting a flaw that could be introduced by model vertical mixing parameterization, atmospheric forcing, or the data assimilation method. To investigate the particular reason for this discrepancy, the sensitivity tests (mode on/off) on each of the possible causes should be provided by the GLORYS12 development team.

The significant disagreements between OBS and GLORYS12 are associated with representing the overflow waters along Greenland and the eastern flank of the Reykjanes Ridge. The overflow waters are significantly warmer (by 0.5°C–1°C) and saltier (by 0.03–0.05) in the reanalysis compared to observations. This is a matter of the fact that the Argo array does not cover the ocean below 2,000 m; thus, GLORYS12 is not directly constrained over these depths by observations, and important model biases persist.

Year-to-year variability revealed by OBS is also relatively well captured by GLORYS12. Linear trends show similar patterns, revealing a dipole-like structure in both T and S with cooling and freshening within and above the main thermocline (the upper thermocline boundary is 27.5 in the ENA above the 27.70 isopycnal), as well as warming and salinification in the deep ocean. The most substantial disagreement in trends is found in the region of overflows. The analysis of correlations calculated at every point of the section demonstrates that GLORYS12 is more accurate than the two other statistical analyses (ARMOR and ISAS) in representing the instantaneous structure of the ocean in this area.

The upper-ocean (0–700 m) heat content is found to be highly consistent between the three products over the whole period (correlation of GLORYS12, ARMOR, and ISAS with OBS is around 0.9). Also, all three products capture well a strong decrease in OHC during 2013–2015. This decrease is likely associated with diabatic cooling imposed by the atmosphere in the subpolar gyre reported by Josey et al. (2018) for 2013–2016 winters. However, a lesser agreement in OHC is found at greater depth (700–2,000 m), while the cooling in 2013–2015 was also reproduced at these depths. While ARGO floats formally cover the upper 2,000 meters, likely assimilation of only ARGO data is not enough for an accurate representation of ocean state and dynamics below 1,000 m.

The cumulative MVT and MHT were analyzed for three particular years (2010, 2014, and 2015) when LADCP observations were available. The year-to-year spread of MVT and MHT estimates is prominent in all three datasets, being the largest in OBS, and no agreement is found between estimates of MVT in the boundary current and in the central Irminger and Iceland Basins where mesoscale eddies dominate the flow. A reasonable agreement is found in the other parts of the section, i.e., on the Reykjanes Ridge and in the North Atlantic Current branches flowing on both sides of the Rockall Plateau. Large discrepancies in the WBC transport result in disagreement in the total cumulative transports across the section. Nevertheless, GLORYS12 shows the best agreement with OBS compared to the two other products (ISAS15 and ARMOR3D).

The information provided daily over the whole period on the large-scale circulation by the reanalysis is used to explain the origin of large-amplitude signals in the MVT and MHT and demonstrate the benefit of dynamical reanalyzes for understanding local observations.

We conclude that over most of the 59.5°N section, the GLORYS12 reanalysis system can realistically reproduce the mean thermohaline structure of the ocean, except for the region of overflows. This important discrepancy emphasizes the need for deep-Argo floats in the future and the model improvement in representing these processes. The low capability of GLORYS12 to reproduce MVT and MHT in the WBCs and the eddy-dominated regions suggests the necessity of higher resolution altimetry being assimilated in the next generations of GLORYS12. In this respect, the expectations linked to the swath altimetry mission SWOT (Desai et al, 2018) are reassuring but will necessitate a proper adaptation of the data assimilation system. Our hypothesis that the existing ARGO float network is not dense enough to provide an accurate assessment of the OHC below 2,000 m in this region suggests the importance of effort on the deep ARGO floats.

Among the lines of the future development of this study, we would mention an extensive use of observational time series at 59.5°N in the Atlantic for evaluation of an ensemble of ocean reanalyzes, which also include coarse-resolution products such as GLORYS2V4 (Garric et al., 2018), SODA3 (Carton et al., 2018) and ORAS5 (Zuo et al., 2019). This will allow for comparative assessment of different ocean reanalysis products using a single reference data set and can potentially put more light onto the differences in ocean state characteristics revealed by different products in the subpolar North Atlantic. Of specific interest will be the realism of representation of meridional transports at 59.5°N in relatively coarse (eddy-permitting) and high (eddy-resolving) reanalysis products with a focus on ~0.25° ocean reanalyzes (Carton et al. 2018; Garric et al., 2018; Zuo et al., 2019). Note that this problem goes far beyond the role of mesoscale eddies in forming meridional transports and relates to the representation of overflows in high-resolution model configurations (Colombo et al., 2020).

A broader context of interest would also be the analysis of sea ice characteristics, including sea ice export in the Greenland Sea as revealed by GLORYS12 and coarser-resolution products.

Appendix A: Calculation Methods

We give here the details of the calculation of the various metrics used in this study.

Root Mean Square of the differences in T and S fields.

The *root mean square* of the differences between the reanalysis and the observed is calculated as follows from the co-localized data:

$$RMSD_j = \sqrt{\frac{\sum_{i=1}^{N}\left(X_{R_{ij}} - X_{O_{ij}}\right)}{N}} \tag{A1}$$

with $N = 14$ is the number of summers (JJAS) with 59.5°N available observations, i is the time index, j is the index of the measurement point in the section in the two-dimensional (2D) depth-longitude space, X states for temperature or salinity, subscript R is for reanalysis data and O for the observational one.

Correlation of the Temperature and salinity differences (Figure 3c)

OBS and GLORYS12 datasets have been projected on a common grid, so we have a realization of the section on that common longitude-depth grid every year. For each year, calculate the T and S differences between GLORYS and OBS at every longitude-depth point of the common grid. So, we have a time series of 14 values of the differences at every point of the section. Then at every point, we calculate the time-correlation between the temperature differences and the salinity differences. This is the correlation coefficient that is plotted in Figure 3c. When the correlation is positive, it means that positive/negative differences in T go with positive/negative differences in S. In other words, when GLORYS12 is warmer/colder than OBS, it is also saltier/fresher. The differences compensate (at least partially) in density. When correlation is negative, it is the opposite.

The calculation of the ocean heat content of the section is performed using potential temperature in °C, interpolated on the model grid. The OHC is consequently relative to the reference temperature of 0°C. The temperature of each point is first weighted by the volume of the corresponding model grid cell, and all temperature points are then summed up across the section and over a given depth range (e.g., from top to bottom, or from 0 to 700 m):

$$HC = \rho C_p \sum_{i=0}^{X} \sum_{j=0}^{Y} \sum_{k=0}^{Z} T_{ijk} \Delta x \Delta y \Delta \tag{A2}$$

where ρ is the water density (kg·m^{-3}), C_p is the ocean water heat capacity (J·kg^{-1}·K^{-1}), T_{ijk} is the temperature at each point on section, $\Delta x \Delta y \Delta z$is the volume of each grid cell, X, Y, and Z are the number of points in the corresponding direction of. Note that $Y = 1$ in the case of a zonal section.

The cumulative meridional volume transport (MVT), accumulated from West to East starting from the coast of Greenland, is calculated as follows:

$$MVT_I = \sum_{k=0}^{Z} \sum_{i=0}^{I} V_{ik} \Delta x \Delta z \tag{A3}$$

where k and i are the grid-cell indexes in respectively the depth and longitude directions, V_{ik} is the meridional velocity at each grid point, $\Delta x \Delta z$ is the area of the face of the grid-cell, Z is the total number of grid cells in the vertical direction (from surface to bottom), I is the number of grid cell in the zonal direction up to which the transport is accumulated from the western boundary (Greenland).

The calculation of meridional heat transport should be:

$$MHT_I = \rho C_p \sum_{k=0}^{Z} \sum_{i=0}^{I} T_{ik} V_{ik} \Delta x \Delta z \tag{A4}$$

Notations are as in Equation A3, and T is temperature (°C). However, such calculation is not possible for observations as we do not have the vertical velocity profiles V_{ik}.

Therefore, we approximate the MHT by replacing in Equation A4 V_{ik} by the vertically averaged velocity, V_i, derived from the barotropic volume transport. The barotropic velocity is given by:

$$V_i = \frac{1}{H}\left(MVT_I\right) \text{ in the case of observations and} \tag{A5a}$$

$$V_i = \frac{1}{H} \sum_{k=0}^{Z} V_{ik} \text{ for the analyzed fields} \tag{A5b}$$

H is the local depth. The approximated MHT is given by:

$$MHT_I = \rho C_p \sum_{k=0}^{Z} \sum_{i=1}^{I} T_{ik} V_i \Delta x \Delta z \tag{A6}$$

Acknowledgments
The 59.5°N section data were provided by Shirshov Institute of Oceanology, Russian Academy of Sciences, the GLORYS12 reanalysis data are available courtesy of Copernicus Marine Environment Monitoring Center (CMEMS). The authors greatly appreciate the comments and recommendations of the two anonymous reviewers and Jim Carton of the University of Maryland. Their suggestions and criticism helped to improve the first version of the paper considerably. This study was supported by the Ministry of Science and Higher Education of Russian Federation under Agreement #14. W0331.0006, RFBR grant 18-05-00194. Sergey K. Gulev and Sergey Gladyshev also benefited from the RSF grant #20-17-00139. Polina Verezemskaya was also supported by the RSF grant #17-77-20112. Bernard Barnier is supported by Centre National de la Recherche Scientifique.

Data Availability Statement

Datasets for this research are available at https://sail.ocean.ru/60N.

References

Akima, H. (1970). A new method of interpolation and smooth curve fitting based on local procedures. *Journal of the ACM*, *17*(4), 589–602

Balmaseda, M., Hernandez, F., Storto, A., Palmer, M., Alves, O., Shi, L., et al. (2015). The Ocean Reanalyzes Intercomparison Project (ORA-IP). *Journal of Operational Oceanography*, *8*, s80–s97. https://doi.org/10.1080/1755876X.2015.1022329

Balmaseda, M. A., Trenberth, K. E., & Källén, E. (2013). Distinctive climate signals in reanalysis of global ocean heat content. *Geophysical Research Letters*, *40*, 1754–1759. https://doi.org/10.1002/grl.50382

Cabanes, C., Grouazel, A., von Schuckmann, K., Hamon, M., Turpin, V., Coatanoan, C., et al. (2013). The CORA dataset: Validation and diagnostics of in-situ ocean temperature and salinity measurements. *Ocean Science*, *9*, 1–18

Carton, J. A., Chepurin, G. A., & Chen, L. (2018). SODA3: A new ocean climate reanalysis. *Journal of Climate*, *31*, 6967–6983. https://doi.org/10.1175/JCLI-D-18-0149.1

Carton, J. A., Penny, S. G., & Kalnay, E. (2019). Temperature and salinity variability in soda3, ECCO4r3, and ORAS5 ocean reanalyzes, 1993–2015. *Journal of Climate*, *32*, 2277–2293. https://doi.org/10.1175/JCLI-D-18-0605.1

Chelton, D. B., deSzoeke, R. A., Schlax, M. G., El Naggar, K., & Siwertz, N. (1998). Geographical variability of the first baroclinic Rossby radius of deformation. *Journal of Physical Oceanography*, *28*, 433–460. https://doi.org/10.1175/1520-0485(1998)028<0433:gvotfb>2.0.co;2

Colombo, P., Barnier, B., Penduff, T., Chanut, J., Deshayes, J., Molines, J. M., et al. (2020). Representation of the Denmark Strait overflow in a z-coordinate eddying configuration of the NEMO (v3. 6) ocean model: Resolution and parameter impacts. *Geoscientific Model Development*, *13*(7), 3347–3371.

D'Addezio, J. M., Jacobs, G. A., Yaremchuk, M., & Souopgui, I. (2020). Submesoscale eddy vertical covariances and dynamical constraints from high-resolution numerical simulations. *Journal of Physical Oceanography*, *50*(4), 1087–1115.

Daniault, N., Mercier, H., Lherminier, P., Sarafanov, A., Falina, A., Zunino, P., et al. (2016). The Northern North Atlantic Ocean mean circulation in the early 21 century//Progr. *Oceanography*, *146*, 142–158. https://doi.org/10.1016/j.pocean.2016.06.007

Dee, D. P., Uppala, S. M., Simmons, A. J., Berrisford, P., Poli, P., Kobayashi, S., et al. (2011). The ERA-Interim reanalysis: Configuration and performance of the data assimilation system. *Quarterly Journal of the Royal Meteorological Society*, *137*(656), 553–597. https://doi.org/10.1002/qj.828

Desai, S., Fu, L. L., Cherchali, S., Vaze, P., Donlon, C. J., Martin, M., et al. (2018). *Tech. Rep. JPL D-61923. National aeronautics and space administration, jet propulsion laboratory*. Remote Sensing of the Environment. Surface Water and Ocean Topography Mission (SWOT) project science requirements document. The Operational Sea Surface Temperature and sea ice Analysis (OSTIA). https://doi.org/10.1016/j.rse.2010.10.0172011

Donlon, C. J., Martin, M., Stark, J., Roberts-Jones, J., Fiedler, E., & Wimmer, W. (2012). The operational sea surface temperature and sea ice analysis (OSTIA) system. *Remote Sensing of Environment*, *116*, 140–158.

DRAKKAR Group, Treguier, A. M., Barnier, B., Blaker, A. T., Biastoch, A., Böning, C. W., Coward, A. J., et al. (2014). DRAKKAR: Developing high-resolution ocean components for European Earth system models. *CLIVAR Exchanges Newsletter*, *64*.

Etling, D., Hansen, D., & Jürrens, R. (1993). The development of mushroom-like vortices from shear flow instabilities. *Dynamics of Atmospheres and Oceans*, *20*(1–2), 107–126. https://doi.org/10.1016/0377-0265(93)90050-h

Ezraty, R., Girard-Ardhuin, F., Piolle, J. F., Kaleschke, L., & Heygster, G. (2007). *Arctic and Antarctic sea ice concentration and Arctic sea ice drift estimated from Special Sensor Microwave data, User's Manual*. CERSATVersion 2.1.

Falina, A., Sokov, A., & Sarafanov, A. (2007). Variability and renewal of Labrador Sea Water in the Irminger basin in 1991–2004. *Journal of Geophysical Research*, *112*, C01006. https://doi.org/10.1029/2005JC003348

Fedorov, K. N., Ginsburg, A. I., & Kostianoy, A. G. (1989). Modelling of "mushroom-like" currents (vortex dipoles) in a laboratory tank with rotating homogeneous and stratified fluids. In *Elsevier Oceanography Series* (Vol. 50, pp. 15–24). Elsevier. https://doi.org/10.1016/s0422-9894(08)70174-0

Fedorov, K. N., & Ginzburg, A. (1986). Mushroom-like' currents (vortex dipoles) in the ocean and in a laboratory tank. *Annales Geophysicae*, *4*, 507–516.

Ferry, N., Parent, L., Garric, G., Barnier, B., & Jourdain, N. C. (2010). Mercator global eddy permitting ocean reanalysis GLORYS1V1: Description and results. *Mercator-Ocean Quarterly Newsletter*, *36*, 15–27.

Gaillard, F., Reynaud, T., Thierry, V., Kolodziejczyk, N., & von Schuckmann, K. (2016). In-situ based reanalysis of the global ocean temperature and salinity with ISAS: Variability of the heat content and steric height. *Journal of Climate*, *29*(4), 1305–1323. https://doi.org/10.1175/JCLI-D-15-0028.1

García-Ibáñez, M. I., Pardo, P. C., Carracedo, L. I., Mercier, H., Lherminier, P., Rios, A. F., & Perez, F. F. (2015). Structure, transports and transformations of the water masses in the Atlantic Subpolar Gyre. *Progress in Oceanography*, *135*, 18–36.

Garric, G., Parent, L., Greiner, E., Drévillon, M., Hamon, M., Lellouche, J. M., et al. (2018). In E. Buch, V. Fernandez, G. Nolan, & D. Eparkhina (Eds.), *Performance and quality assessment of the global ocean eddy-permitting physical reanalysis GLORYS2V4 operational oceanography serving sustainable marine development. Proceedings of the eight EuroGOOS international conference. 3-5 October 2017, Bergen, Norway* (p. 516). EuroGOOS (ISBN:978-2-9601883-3-2).

Gladyshev, S. V., Gladyshev, V. S., Gulev, S. K., & Sokov, A. V. (2016). Anomalously deep convection in the irminger sea during the winter of 2014–2015. *Doklady Earth Sciences*, *469*(1), 766–770. https://doi.org/10.1134/S1028334X16070229

Gladyshev, S. V., Gladyshev, V. S., Gulev, S. K., & Sokov, A. V. (2017). Subpolar mode water classes in the northeast Atlantic: Interannual and long-term variability. *Doklady Earth Sciences*, *476*(2), 1203–1206. https://doi.org/10.1134/S1028334X17100166

Gladyshev, S. V., Gladyshev, V. S., Gulev, S. K., & Sokov, A. V. (2018). Structure and variability of the meridional overturning circulation in the North Atlantic subpolar gyre, 2007–2017. *Doklady Earth Sciences*, *483*(2), 1524–1527. https://doi.org/10.1134/S1028334X18120024

Gladyshev, S. V., Gladyshev, V. S., Klyuvitkin, A. A., & Gulev, S. K. (2019). A new look at the water exchange between the arctic and the north Atlantic in the Iceland Basin. *Doklady Earth Sciences*, *485*(2), 401–404. https://doi.org/10.1134/S1028334X19040020

Good, S. A., Martin, M. J., & Rayner, N. A. (2013). EN4: Quality-controlled ocean temperature and salinity profiles and monthly objective analyses with uncertainty estimates. *Journal of Geophysical Research: Oceans*, *118*, 6704–6716. https://doi.org/10.1002/2013JC009067

Guinehut, S., Dhomps, A.-L., Larnicol, G., & Le Traon, P.-Y. (2012). High-resolution 3D temperature and salinity fields derived from in situ and satellite observations. *Ocean Science*, *8*(5), 845–857. https://doi.org/10.5194/os-8-845-2012

Hamon, M., Greiner, E., Le Traon, P.-Y., & Remy, E. (2019). Impact of multiple altimeter data and mean dynamic topography in a global analysis and forecasting system. *Journal of Atmospheric and Oceanic Technology*, *36*, 1255–1266. https://doi.org/10.1175/JTECH-D-18-0236.1

Josey, S. A., Hirschi, J. J.-M., Sinha, B., Duchez, A., Grist, J. P., & Marsh, R. (2018). The recent atlantic cold anomaly: Causes, consequences, and related phenomena. *Annual Review of Marine Science*, *10*(1), 475–501. https://doi.org/10.1146/annurev-marine-121916-063102

Kolodziejczyk, N., Prigent-Mazella, A., & Gaillard, F. (2017). ISAS-15 temperature and salinity gridded fields. *SEANOE*. https://doi.org/10.17882/52367

Lellouche, J.-M., Greiner, E., Le Galloudec, O., Garric, G., Regnier, C., Drevillon, M., et al. (2018). Recent updates to the Copernicus Marine Service global ocean monitoring and forecasting real-time 1⁄12° high-resolution system. *Ocean Science*, *14*, 1093–1126. https://doi.org/10.5194/os-14-1093-2018

Madec, G., & The NEMO team. (2016). *NEMO ocean engine. Note du Pôle de modélisation*. Institut Pierre-Simon Laplace (IPSL), France. No 27 ISSN No 1288-1619.

Masina, S., Storto, A., Ferry, N., Valdivieso, M., Haines, K., Balmaseda, M., et al. (2015). *An ensemble of eddy-permitting global ocean reanalyzes from the MyOcean project* (Vol. 49, pp. 813–841). https://doi.org/10.1007/s00382-015-2728-5

Meyssignac, B., Boyer, T., Zhao, Z., Hakuba, M. Z., Landerer, F. W., Stammer, D., et al. (2019). Measuring global ocean heat content to estimate the earth energy imbalance. *Frontiers in Marine Science*, *6*, 432. https://doi.org/10.3389/fmars.2019.00432

Mied, R. P., Lindemann, G. J., & McWilliams, J. C. (1991). The generation and evolution of mushroom-like vortices. *Journal of Physical Oceanography*, *21*(4), 489–510. https://doi.org/10.1175/1520-0485(1991)021<0489:tgaeom>2.0.co;2

Mulet, S., Rio, M.-H., Mignot, A., Guinehut, S., & Morrow, R. (2012). A new estimate of the global 3D geostrophic ocean circulation based on satellite data and in-situ measurements. *Deep Sea Research Part II*, *77–80*(0), 70–81. https://doi.org/10.1016/j.dsr2.2012.04.012

Palmer, M. D., Roberts, C. D., Balmaseda, M., Chang, Y. S., Chepurin, G., Ferry, N., et al. (2017). Ocean heat content variability and change in an ensemble of ocean reanalyses. *Climate Dynamics*, *49*(3), 909–930.

Pujol, M. I., Faugère, Y., Taburet, G., Dupuy, S., Pelloquin, C., Ablain, M., & Picot, N. (2016). DUACS DT2014: The new multi-mission altimeter data set reprocessed over 20 years. *Ocean Science*, *12*(5), 1067–1090.

Rio, M. H., Mulet, S., & Picot, N. (2014). Beyond GOCE for the ocean circulation estimate: Synergetic use of altimetry, gravimetry, and in situ data provides new insight into geostrophic and Ekman currents. *Geophysical Research Letters*, *41*, 8918–8925. https://doi.org/10.1002/2014GL061773

Roemmich, D., & Argo Steering Team. (2009). Argo: The challenge of continuing 10 years of progress. *Oceanography*, *22*(3), 46–55.

Sarafanov, A., Falina, A., Mercier, H., Sokov, A., Lherminier, P., Gourcuff, C., et al. (2012). Mean full-depth summer circulation and transports at the northern periphery of the Atlantic Ocean in the 2000s. *Journal of Geophysical Research*, *117*, C011014. https://doi.org/10.1029/2011JC007572

Sarafanov, A., Falina, A., Sokov, A., & Demidov, A. (2008). Intense warming and salinification of intermediate waters of southern origin in the eastern subpolar North Atlantic in the 1990s to mid-2000s. *Journal of Geophysical Research*, *113*(C12). https://doi.org/10.1029/2008JC004975

Sarafanov, A., Falina, A., Sokov, A., Zapotylko, V., & Gladyshev, S., (2018). Ship-based monitoring of the northern north Atlantic Ocean by the Shirshov Institute of Oceanology. The main results. In *Ship-based monitoring of the northern North Atlantic ocean by the Shirshov Institute of Oceanology*. The Ocean in Motion (pp. 415–427). Springer Oceanography. https://doi.org/10.1007/978-3-319-71934-4_25

Sarafanov, A., Mercier, H., Falina, A., Sokov, A., & Lherminier, P. (2010). Cessation and partial reversal of deep water freshening in the northern North Atlantic: Observation-based estimates and attribution. *Tellus*, *62*(1), 80–90. https://doi.org/10.1111/j.1600-0870.2009.00418.x

Shi, L., Alves, O., Wedd, R., Balmaseda, M. A., Chang, Y., Chepurin, G., et al. (2017). Assessment of upper ocean salinity content from the Ocean Reanalyzes Inter-comparison Project (ORA-IP). *Climate Dynamics*, *49*, 1009–1029. https://doi.org/10.1007/s00382-015-2868-7

Simpson, J. J., & Lynn, R. J. (1990). A mesoscale eddy dipole in the offshore California Current. *Journal of Geophysical Research*, *95*(C8), 13009–13022. https://doi.org/10.1029/jc095ic08p13009

Storto, A., Alvera-Azcárate, A., Balmaseda, M. A., Barth, A., Chevallier, M., Counillon, F., et al. (2019). Ocean reanalyzes: Recent advances and unsolved challenges. *Frontiers of Marine Sciences*, *6*, 418. https://doi.org/10.3389/fmars.2019.00418

Storto, A., Masina, S., Balmaseda, M., Guinehut, S., Xue, Y., Szekely, T., et al. (2017). Steric sea level variability (1993–2010) in an ensemble of ocean reanalyzes and objective analyses. *Climate Dynamics*, *49*, 709–729. https://doi.org/10.1007/s00382-015-2554-9

Szekely, T., Gourrion, J., Pouliquen, S., & Reverdin, G. (2016). CORA, coriolis, ocean dataset for reanalysis. *SEANOE*. https://doi.org/10.17882/46219

Thurnherr, A. M. (2010). A practical assessment of the errors associated with full-depth LADCP profiles obtained using Teledyne RDI Workhorse acoustic Doppler current profilers. *Journal of Atmospheric and Oceanic Technology*, *27*(7), 1215–1227. https://doi.org/10.1175/2010jtecho708.1

Våge, K., Pickart, R. S., Spall, M. A., Valdimarsson, H., Jónsson, S., Torres, D. J., & Eldevik, T. (2011). Significant role of the North Icelandic Jet in the formation of Denmark Strait overflow water. *Nature Geoscience*, *4*(10), 723–727.

Valdivieso, M., Haines, K., Balmaseda, M., Chang, Y.-S., Drevillon, M., Ferry, N., et al. (2017). An assessment of air–sea heat fluxes from ocean and coupled Reanalyzes. *Climate Dynamics*, *49*, 983–1008. https://doi.org/10.1007/s00382-015-2843-3

Visbeck, M. (2002). Deep velocity profiling using lowered acoustic Doppler current profilers: Bottom track and inverse solutions. *Journal of Atmospheric and Oceanic Technology*, *19*(5), 794–807. https://doi.org/10.1175/1520-0426(2002)019<0794:dvpula>2.0.co;2

von Schuckmann, K., Le Traon, P., Smith, N., Pascual, A., Djavidnia, S., GattusoZuo, J. H., et al. (2019). Copernicus marine service ocean state report, issue 3. *Journal of Operational Oceanography*, *12*, S1–S123. https://doi.org/10.1080/1755876X.2019.1633075

von Schuckmann, K., Le Traon, P.-Y., Alvarez-Fanjul, E., Axell, L., Balmaseda, M., Breivik, L.-A., et al. (2016a). The copernicus marine environment monitoring service ocean state report, *Journal of Operational Oceanography*. *9*, s235–s320. https://doi.org/10.1080/1755876X.2016.1273446

von Schuckmann, K., Le Traon, P.-Y., Smith, N., Pascual, A., Brasseur, P., Fennel, K., et al.(2018). Copernicus marine service ocean state report. *Journal of Operational Oceanography*. *11*, pp. s1–s142. https://doi.org/10.1080/1755876X.2018.1489208

von Schuckmann, K., Palmer, M. D., Trenberth, K. E., Cazenave, A., Chambers, D., Champollion, N., et al. (2016b). An imperative to monitor Earth'senergy imbalance. *Nature Climate Change*, *6*, 138–144. https://doi.org/10.1038/NCLIMATE2876

Vortmeyer-Kley, R., Gräwe, U., & Feudel, U. (2016). Detecting and tracking eddies in oceanic flow fields: A Lagrangian descriptor based on the modulus of vorticity. *Nonlinear Processes in Geophysics*, *23*(4), 159–173.

Xue, Y., Balmaseda, M. A., Boyer, T., Ferry, N., Good, S., Ishikawa, I., et al. (2012). A comparative analysis of upper-ocean heat content variability from an ensemble of operational ocean reanalyzes. *Journal of Climate*, *25*, 6905–6929. https://doi.org/10.1175/jcli-d-11-00542.1

Zuo, H., Alonso Balmaseda, M. A., Tietsche, S., Mogensen, K., & Mayer, M. (2019). The ECMWF operational ensemble reanalysis-analysis system for ocean and sea-ice: A description of the system and assessment. *Ocean Science*, *15*, 779–808. https://doi.org/10.5194/os-15-779-2019

Zuo, H., Balmaseda, M. A., & Mogensen, K. (2015). The new eddy-permitting ORAP5 ocean reanalysis: Description, evaluation and uncertainties in climate signals. *Climate Dynamics*, *49*, 791–811. https://doi.org/10.1007/s00382-015-2675-1